

A
Dissertation Report
On

Analysis of Motorcycle Model for Road Bumps

Submitted in Partial Fulfillment of the Requirements for the Award of Degree of

Master of Technology

In

Design Engineering

By

MANGESH JADHAV

2014PDE5010

Under the Guidance of

Dr. T.C. GUPTA

Associate Professor

Department of Mechanical Engineering

MNIT, Jaipur



**DEPARTMENT OF MECHANICAL ENGINEERING
MALAVIYA NATIONAL INSTITUTE OF TECHNOLOGY
JAIPUR-302017 (RAJASTHAN) INDIA
JUNE 2016**



DEPARTMENT OF MECHANICAL ENGINEERING
MALAVIYA NATIONAL INSTITUTE OF TECHNOLOGY
JAIPUR-302017 (RAJASTHAN) INDIA

CERTIFICATE

This is certified that the dissertation report entitled “**Analysis of Motorcycle Model for Road Bumps**” prepared by **MANGESH JADHAV** (ID-2014PDE5010), in the partial fulfillment of the award of the Degree **Master of Technology in Design Engineering** of Malaviya National Institute of Technology Jaipur is a record of bonafide research work carried out by him under my supervision and is hereby approved for submission. The contents of this dissertation work, in full or in parts, have not been submitted to any other Institute or University for the award of any degree or diploma.

Mangesh Jadhav
2014PDE5010

This dissertation report is hereby approved for submission.

Date:

Dr. T.C. Gupta

Place:

Associate Professor
Department of Mechanical Engineering
MNIT, Jaipur, India

Acknowledgement

I would like to express my heartfelt thanks and profound gratitude to my supervisor **Dr T.C. Gupta** who provided me with generous guidance and proper direction which enabled me to complete this dissertation work. I am also grateful to **Dr. Himanshu Chaudhary, Dr. Dinesh Kumar** and **Dr. Amit Singh** for their presence and encouragement.

I would like to convey my thanks to **Manoj Gupta** for inspiring and helping me with his deep insights in completing this dissertation work. A vote of thanks is due to **Ajit Singh** who has always provided me with honest and precious advice.

Lastly, I would like to give the highest regards to my family and the Providence. My faith in them has always been rewarded beyond measure.

Mangesh Jadhav
Design Engineering
2014PDE5010

Abstract

Two wheelers especially Motorcycles are an important means of transportation throughout the world. Dynamic analysis of motorcycles is important from the point of view of safety and comfort of the rider. Motorcycle dynamic analysis is classified into two main types: in-plane and out-plane motion. This thesis focuses on the in-plane motion of a motorcycle. Various motorcycle models with different degrees of freedom (DOF) are analysed. The 4 DOF Model is analysed with road excitation and the Frequency Response (FRF) plots are generated for relative coordinates. A 6 DOF Model of motorcycle is subjected to excitations from a C-grade road profile and the vertical accelerations of the sprung mass and the passenger are analysed using Matlab and Simulink software. The 6 DOF model's response is also analysed after subjecting it to real time speed bump data and various inferences are drawn. LSim and LTiview are used for displaying results. Single sided PSD for response to a realistic speed bump profile is plotted. Also a comparison of triangular bump PSD is performed for both 6 DOF and 5 DOF Models which provides useful insights.

Contents

ACKNOWLEDGEMENT	iii
Abstract	iv
List of figures	vi
List of tables	viii
Nomenclature	ix
Chapter 1 Introduction	1
1.1 Background	1
1.2 Motorcycle Dynamics	3
1.3 Traffic Calming Devices	4
Chapter 2 Literature Review	6
2.1 Research Objective	11
Chapter 3 Methodology	12
3.1 4 DOF Motorcycle Model	12
3.1.1 Equation of motion in absolute coordinates	15
3.1.2 Motorcycle response to road profile	17
3.1.3 Calculating FRF Matrix in absolute coordinates	18
3.2 6 DOF Motorcycle Model	20
3.2.1 C-grade road input	28
3.2.2 State space formulation of the 6 DOF Model	26
3.2.3 Generating C grade road profile for front wheel	30
3.2.4 Generating C grade road profile for rear wheel	31
3.2.5 6 DOF model for C grade road in Simulink	32
3.3 Realistic Bump (problem statement)	34
3.3.1 6 DOF model for realistic bump in Simulink	39
3.4 Triangular bump (5 DOF PSD)	37
Chapter 4 Results and Discussion	40
4.1 4 DOF Model verification	40
4.2 6 DOF with C grade road input	43
4.3 6 DOF Model with realistic speed bump	48
4.4 Comparison of 5 DOF & 6 DOF for triangular bump	52
Chapter 5 Conclusions and Future work	53
References	55
Appendix	61

List of figures

Figure 1.1: 1894 Hildebrand and Wolfmuller (from[26])	1
Figure 1.2: 2016 Yamaha R1 (from[27])	2
Figure 1.3: Harley-Davidson Iron 883 (from[28])	2
Figure 1.4: Husqvarna FE 501 (Off-road) (from[29])	2
Figure 1.5: In-plane modes of vibration of a motorcycle (from[2])	3
Figure 1.6: Speed bump(from[30])	4
Figure 1.7: Speed hump(from[31])	4
Figure 3.1: Reduced Suspension for 4 DOF model(from[2])	12
Figure 3.2: 4 DOF Motorcycle Model (Abs Co-ordinates)(from[24])	13
Figure 3.3: 4 DOF Motorcycle Model (Relative Co-ordinates)(from[2])	15
Figure 3.4: 6 DOF Motorcycle Model	20
Figure 3.5: State space block explanation(from[25])	23
Figure 3.6: Generating Input for the front tyre	28
Figure 3.7: Generating input for the rear tyre	29
Figure 3.8: Lag values in the transport delay block	30
Figure 3.9: Simulink Model for 6 DOF motorcycle model	31
Figure 3.10: Entering A,B,C,D values in the state space block	31
Figure 3.11: Design Data for Speed bump (from [23])	33
Figure 3.12: Height vs Width plot in Matlab	33
Figure 3.13: Realistic bump for front wheel	34
Figure 3.14: Realistic bump for rear wheel	34
Figure 3.15: Linear Simulation Tool	35
Figure 3.16: Procedure for data import	36
Figure 3.17: Plot configurations of LTIVIEW	36
Figure 3.18: Simulink model for 6 DOF Motorcycle (Realistic Bump)	39
Figure 3.19: Triangular bump (from [3])	40
Figure 3.20: Triangular bump from Matlab	40
Figure 3.21: Triangular bump for front wheel	38

Figure 3.22: Triangular bump for rear wheel	41
Figure 3.23: Simulink Model for triangular bump	42
Figure 4.1: Frequency Response for rear sprung mass	43
Figure 4.2: Frequency Response of front sprung mass	44
Figure 4.3: Frequency Response Function of rear unsprung mass	45
Figure 4.4: Frequency Response Function of front unsprung mass	45
Figure 4.5: Front wheel input obtained from Simulink	46
Figure 4.6: Front wheel input from reference [4]	46
Figure 4.7: Rear wheel input obtained from Simulink	47
Figure 4.8: Rear wheel input from reference [4]	47
Figure 4.9: Vertical acceleration of Sprung mass (Simulink Scope)	48
Figure 4.10: Vertical acceleration of Sprung mass from[4]	48
Figure 4.11: Vertical acceleration of Passenger (Simulink Scope)	49
Figure 4.12: Vertical acceleration of Passenger from [4]	49
Figure 4.13: Force acting on passenger	50
Figure 4.14: Passenger acceleration	51
Figure 4.15: Sprung mass acceleration	52
Figure 4.16: Vertical force acting on the passenger	53
Figure 4.17: PSD for the passenger acceleration for 6 DOF	53
Figure 4.18: lsim and bode plot of bump response	54
Figure 4.19: Rider PSD for 5 and 6 DOF comparison	55

List of tables

Table 3.1 Motorcycle parameters for 4 DOF model from [2]	14
Table 3.2 Parameters for 6 DOF Motorcycle model from [4]	27

Nomenclature

4 DOF MODEL

p	wheelbase
b	distance from the CG to the rear wheel
m	sprung mass
m_f	Front unsprung mass
m_r	Rear unsprung mass
I_{yg}	Pitch Moment of Inertia
k_f	Reduced stiffness of front suspension
k_r	Reduced stiffness of rear suspension
c_f	Reduced damping of the front suspension
c_r	Reduced damping of the rear suspension
k_{pf}	Front tyre stiffness
k_{pr}	Rear tyre stiffness
c_{pf}	Front tyre damping
c_{pr}	Rear tyre damping

6 DOF Model

m_p	Passenger mass
k_p	Reduced stiffness of the passenger
c_p	Reduced damping of the passenger
m_g	Mass of engine
k_g	Stiffness of engine

c_g	Damping of engine
m_c	Sprung mass
I_c	Pitch Moment of Inertia
m_{uf}	Front unsprung mass
m_{ur}	Rear unsprung mass
k_{mf}	Front suspension stiffness
k_{mr}	Rear suspension stiffness
c_{mf}	Front suspension damping
c_{mr}	Rear suspension damping
k_{uf}	Front tyre stiffness
k_{ur}	Rear tyre stiffness
l_f	Distance of front axle from the C.G.
l_r	Distance of rear axle from the C.G.
l_p	Distance of passenger from the C.G.
l_g	Distance of engine from the C.G.

Acronyms

DOF Degree of Freedom

Chapter 1 Introduction

1.1 Background

A motorcycle may be defined as a two-wheeled (or if attached with a sidecar, three-wheeled) vehicle propelled by an Internal Combustion Engine and resembling a bicycle, which is usually larger and heavier and has a seating arrangement for two persons.

Motorcycle design varies for different purposes such as long distance travel, cruising, urban commuting, leisure and recreation such as cruising and sports motorcycles which can be either racing or off-road. In the year 1894, Hildebrand and Wolfmuller became the first bike that was series produced.



Figure1.1: 1894 Hildebrand and Wolfmuller [26]

Classifying motorcycles on the basis of steering rake angle we can classify them as racing, cruising, and off-road motorcycles.

Racing bikes are by design made as light-weight as possible to improve the power to weight ratio for achieving high speeds. Some professional racing bikes are made intentionally unstable for lightning fast direction changes. Racing Bikes usually have a fairing which puts more weight on the front. This leads to better braking performance in a straight line. They are also equipped with dual rotor disc brakes. Advanced electronics such as traction control, ABS (Anti-lock braking system), wheelie control, wet modes, launch control may be part of the racing package for better safety. To reduce drag they also have visors or wind deflectors. Inline fours and V-twin Engines dominate the engines used for racing. The 2016 Yamaha R1 (figure 1.2) has a cross plane crankshaft with ride by wire throttle



Figure 1.2: 2016 Yamaha R1 [27]

Cruisers have a higher rake angle. Due to this, they possess excellent straight line stability. Their forward set design reduces fatigue and allows them to carry heavy loads for a longer duration. Engines used for cruising usually have a large displacement V-twin engine tuned for low-end torque which in turn facilitates a lesser number of gearshifts. Figure 1.3 shows a cruising motorcycle



Figure 1.3: Harley Davidson Iron 883 [28]

Off-road motorcycles need to be light-weight and have external body parts that can be easily replaced. They need to have a chassis strong enough to withstand shocks in the rough terrain. The front suspension also has to have a longer travel to prevent shocks to the rider. Figure 1.4 shows an off-road motorcycle.



Figure 1.4: Husqvarna FE 501 (Off-road) [29]

1.2 Motorcycle Dynamics:

A motorcycle as in the case of any motorised vehicle needs to conform to a set of comfort and safety criteria. To accomplish these aspects require meticulous study of dynamic behaviour of the motorcycle.

From a dynamic point of view, a motorcycle can be described as a rigid body connected to two rotating members (wheels) with elastic systems (spring and damper suspension arrangement). Certain assumptions about the motorcycle lead to a simplified dynamic model which enables us to obtain performance of the motorcycle. Once the conditions of motorcycle behaviour testing are decided, simplifying assumptions are made.

The two general kinds of motion a motorcycle performs is as follows:

- I. In-plane motion: It occurs when the motorcycle travels on a straight road and is assumed to be lying all the time in the vertical plane. In-plane modes include the motion of frame, suspension masses and even wheels. For further work in this thesis, the criteria assumed is in-plane motion.

Sprung mass has two types of modes about its centre. The first mode also called bounce mode represents the pure vertical translation and the second mode called as pitch mode represents pure rotation about the centre of gravity(usually on the sprung mass). Bounce and Pitch motion for in-plane has been shown in figure 1.5 In-plane modes occur in the range of 300-400 Hz. The modes for unsprung masses are called front and rear hop.

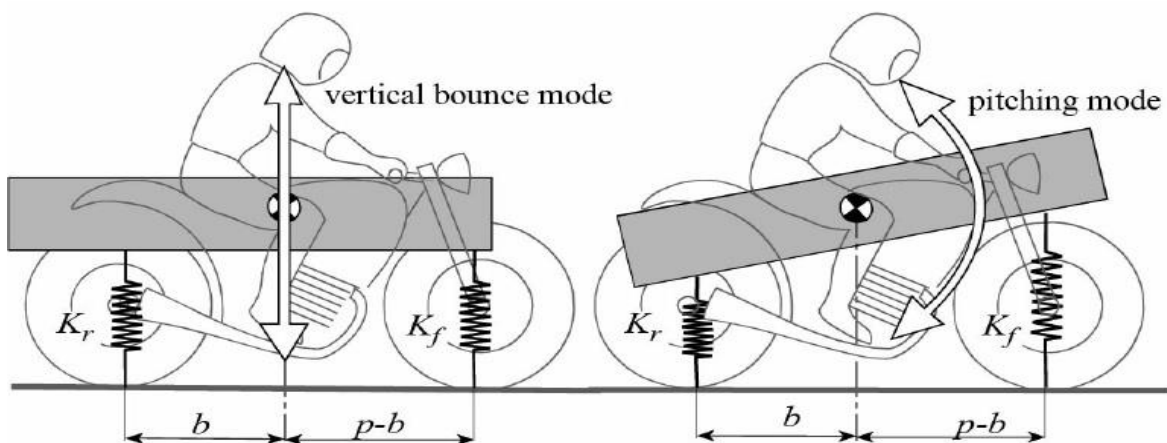


Figure 1.5: In-plane modes of vibration of a motorcycle [2]

II. Out-of-plane motion: It represents the out of plane modes such as capsize, weave and steering wobble. Its analysis involves roll, yaw, steering angles and lateral displacement of the steering head. The out of plane motion modes are detailed briefly as follows:

Capsize is a type of manoeuvre, non-oscillating by nature. It is used controllably by the rider for initiating a turn.

Weave describes a slow oscillation which occurs between the lean axis and the steering axis. It affects the rear part of the motorcycle the most.

Wobble also called tank-slapper, is a violent oscillation of the handlebar about its steering axis. Wobble is very difficult for the rider to control and thus can cause accidents. Wobble is very difficult to predict, but instances of wobble can be reduced using a steering damper.

Out-of-plane modes occur in the range of 100-200 Hz.

The in-plane modes are related to the comfort and stability of the motorcycle. Also, the in-plane modes with larger displacements dominate, which holds true in the study of responses to speed bumps.

Thus, in-plane motion holds more relevance in the study vis a vis speed bumps.

1.3 Traffic Calming Devices

Speed Bumps are ‘traffic calming’ devices that use vertical deflection to slow motor vehicle traffic. Traffic calming devices include speed bumps and speed humps.

Speed Bumps: The first speed bump was implemented in New York in 1906. They can be made of a variety of materials including concrete, asphalt, plastic or vulcanized rubber. Traditionally most vertical displacement devices have been constructed from asphalt or concrete. Due to rigidity and durability of these materials, these have more permanence. However, cement and asphalt are very difficult to shape and form into precise dimensions. Figure 1.6 shows a typical speed bump.

Speed Humps: It is a rounded ‘traffic calming’ device used to reduce vehicle speed and volume. The purpose of a hump is also to reduce vehicle speed and volume. The purpose of hump is to slow traffic, and they are often installed in series. Common shapes are parabolic, circular and sinusoidal. They have greater traverse distance as compared to speed bump and lesser height. They have a smoother profile as compared to speed bumps and permit higher velocities.

Figure 1.7 shows a typical speed hump

Speed bumps slow cars to 8 -16 kmph, humps slow cars to 24-32 kmph.



Figure 1.6: Speed bump [30]



Figure 1.7: Speed hump [31]

- Speed bumps cause an increase in fuel consumptions and emissions.
- They also cause increased wear on brakes, engine and suspension components.
- Speed bumps slow down the response of emergency services. It is estimated that speed bumps slow down fire trucks by 3-5 seconds and ambulances with the patient on board by up to 10 seconds.
- In [9] by Serbian author Vlastimir Dedovic studied the effects of speed bumps on passenger health. Speed bumps have health effects such as:
They incite sensation of discomfort, reduce work capacity.
- Speed bumps affect the musculo-skeleton interface of the spine. This includes pain in shoulders, neck, upper part of back (cervical) and lower back pain (lumbar).
- In a recent case in the U.K, five passengers travelling in a double decker bus developed spinal cord injuries when their bus went over a speed bump.
- The effect of speed bump is particularly more for passengers seated towards the rear.
- While speed bumps reduce accidents by restricting speed, they subject the passenger to high-intensity vibration. Repeated exposure to such high-intensity vibration causes injury to the spinal column. Considering the relevance of speed bumps on health and suspension components; this thesis deals with response of motorcycle to road roughness and a realistic road bump.

Chapter 2 Literature Review

C.Fuhrer et al. [1] developed the multi-body system formulation for an in-plane vertical truck model with a non-linear suspension. Equations of motion are formulated using Newton & Euler equations, and a holonomic (position) constraint is applied to the system. The DAE (i.e., Differential Algebraic Equations) obtained are subjected to numerical integration using DASSL (Differential Equation System Solver) for a displacement input. Altering RTOL and ATOL they have tried to reduce ‘drift off’ effect & the simulation system road. Thus, they presented a different approach to the truck-model problem.

Luis Ricardo [2] in his thesis approaches motorcycle dynamics with a non-linear stochastic approach. He states the key elements as model, excitation from the road & the response of the system. Random processes and Gaussian probability distribution function are also described. White Noise approach has used to calculate PSD. Monte Carlo Simulation has been used for the non-linear problem. A 4 DOF motorcycle model with reduced suspension is used. The concept of lag and wheelbase filtering is explained. Road excitation assumed is sinusoidal initially. Auto- Regressive filters are used to generate the road surface from its PSD.FRF i.e., (Frequency Response Function) for absolute as well as relative coordinates are plotted. Acceleration PSD response for sprung mass modes (pitch and bounce) are plotted. PSD results are in the time domain as well as frequency domain.

Dongmei Yuan et al. [3] analyzed motorcycle ride comfort based on bump road. A 5 DOF motorcycle model is used. Additional dof as compared to 4 DOF is DOF of the passenger. The equations of motion so formulated are converted to the state space form. The input is a triangular bump. The simulation program gives PSD in the frequency domain graph for speeds ranging from 10km/h to 60 km/h. This data is compared with real life 125 motorcycle test data. It is a notable observation that response has concentrated power at 2.3 Hz.

L.Wu et al. [4] applied semi-active control in a motorcycle model with six degrees of freedom. Front & rear suspensions are modeled as independent local 2 DOF systems. Sprung mass has been treated as a control object. LQG (Linear Quadratic Gaussian) algorithm & Matlab are used.

Simulation results show that simplifying model reduces CPU processing time. Comparison between hierarchical vs. traditional modeling results are discussed.

V.Cossalter, Roberto Lot et al. [5] state that improving the comfort of two wheelers can lead to less fatigue amongst workers which leads to improvement in the safety of ground transport. Acceleration is transformed into frequency domain using FRF. Numerical calculations are performed using FastBike a multibody code. The front and rear FRF are shown using Nyquist plot. Average quality roads are assumed for PSD calculations. The RMS response of the PSD curves are also plotted which helps in understanding comfort indices and also the sensitivity of vibration keeping in mind rider comfort.

Xihong Zou, Zhang et al. [6] analyzed ride comfort using rigid-flexible coupling virtual prototype. The so-prototype is developed with the help of softwares CATIA, Adams and NASTRAN. The pulse input simulation is in the form of a triangular bump. Ride comfort affects the motorcycle part's working life. Using software tools, it is possible to analyse performance before trial and prototype production. The frame data is measured using CMM i.e. coordinate measuring machine. The cad data from CATIA is input into Adams. Bump is simulated for velocities ranging from 10 to 60 km/h. PSD of seat acceleration is plotted vis a vis simulator data.

Tyan, Hong et al. [7] state the methods for generating random road profiles. They state shaping filter method & sinusoidal approximation. Paved asphalt roads are from classes A to D. This paper mentions the procedure to convert PSD to road profile. Using alpha and velocity applied to a linear filter, the authors have given a Simulink program of finding the road profile. The alpha values are available for various grades of roads. They have derived equations for both methods & found time constant of associated transfer function is independent of the grade of road profile.

Dr.D.S.Deshmukh et al. [8] performed vibration analysis of a motorcycle. They say that improper design of motorcycle and its suspension leads to lower back pain of musculoskeletal nature. They have tried to prove that seat acceleration of indian motorcycles is somewhat more as compared to international standard. Vibration from range 4 to 8 Hz causes the chest cavity resonance and is particularly harmful. They have analysed real-time data from Hero Ignitor motorcycle. At two different speeds, the acceleration of rider is measured on four different road profiles. They recommend better design of shock absorbers to prevent vibration effects that cause fatigue and are harmful in the long run.

O.Kropac and P.Mucka[9] explain the effect of bumps and potholes on the vehicle response and the passenger. The obstacle is in the form of a cosine wave with varying height but a fixed height to length ratio. They consider the inplane analysis of a car as well as a three-axle truck. RMS values of the response are also analysed. Road Obstacles in the long term can cause fatigue of critical components. The vertical acceleration acting on the passenger's head in a car is also analysed. They found maximum acceleration depends linearly on the obstacle height. Checking the same model again with non-linear parameters in springs and dampers they found very similar results.

P.Sathiskumar et al. [10] describe modeling and simulation of a 2 DOF quarter car model. They have tested passive, semi-active and active suspension for the same situation. Input is a double road input. Passive Suspension is modeled in Simulink. Sprung and Unsprung mass displacement, as well as suspension deflection, is deduced in the result as a result of a road bump. They finally conclude that using active suspension reduces peak amplitude and the settling time thus finding it to be a superior alternative to passive and semi-active.

Liqiang Jin et al. [11] studied the effects that the in-wheel motor would have on the vehicular ride comfort. The introduction of an in-wheel motor brings with it, an addition in the value of unsprung mass. The vehicle model, in this case, has 11 DOF. It is simulated using Matlab/Simulink. Road tests are performed for corroborating the results. Road excitation in the time domain is usually considered as randomly acting stationary Gaussian process. This paper, authors have considered filtered white noise method. They have assumed a B class pavement for road excitation. The value of Force for different value of unsprung mass is calculated and it is found that increase in unsprung mass has a direct bearing on reducing the passenger comfort. The so-said unsprung masses are bolted on to the wheels. To reduce this phenomenon, authors suggest PID (Proportional Integral Derivative) control with air-suspension to improve comfort.

Jung Feng et al. [12] explain one wheel and four wheel, road time domain model. The deviation between 2 wheel road PSD on the same axle is studied initially. Then they propose a frequency compensation algorithm to correct PSD on the same axle. This algorithm is supplied to road-time domain and is studied via simulation. This procedure and algorithmic efficacy is finally tested by applying on a 7 DOF vehicle model. Also, the irregularities responsible for different dynamic behaviour are analysed and real-time data is plotted. Also a coherence of 4 wheel input is used to describe the relation between left and right wheels on the same axle. They recommend the

installation of a control system to compensate for different road roughness and damper tuning for each application.

S.Narayana et al. [13] consider a 4 DOF car model on a rough road. The suspension springs are hysteretic non-linear in nature. Linear model is modeled using statistical linearization. They seek to optimize the suspension response with respect to suspension stroke and road holding. The results are verified using Monte-Carlo simulation. Half-car model so used bears resemblance to 4 DOF Motorcycle model. The performance index of suspension for different velocities are obtained, and so are RMS values for front and rear tyre deflections.

V.Thomas et al. [14] envisage the use of semi-active suspension over the conventional telescopic one. A passive suspension might not suit all road conditions. Rigid suspension provides with good handling, but soft suspension provides comfort on harsh roads. They suggest a damper which uses pressurized air and whose damping is adjustable depending on road conditions. Using DAQ (Data Acquisition System), they plot the different suspension against pressures. The rigidity or softness of the suspension can be varied according to air pressure. They then compare PSD of semi-active vs. passive suspension for smooth as well as rough roads.

Wu Weiguo et al. [15] analysed the response of landing gear of an airplane at taxiing and impacting phase. A 2 DOF model of landing gear is prepared, and its dynamic equations are established. The unevenness time series is generated using harmony superposition method. The 10000 samples whose interval width is smaller yields displacement response. Statistical Analysis such as mean, mean square, autocorrelation function and PSD are obtained. CPU processing time data, 95% confidence data over the mean are plotted. They finally conclude 10000 samples are enough for comparison between numerical simulation and analytical method. From PSD plot, simulation track is Gaussian random. Even though the input is Gaussian, the response is non-Gaussian.

Zhang et al [16] modeled and simulated time histories for stochastic road excitation. Mathematical modeling is followed by algorithm design and then by simulation realization of the road in the time domain. Three algorithms are used for the same namely harmony super-position, white noise filtration and Inverse FFT (Fast Fourier Transform) based on road spectral PSD are designed and integrated based on MATLAB. For road frequency model, time correlation between the front and rear wheel excitation is considered. They have simulated three grades of roads viz A, B, C grades;

they have proved that the road excitation data generated can be used in the place of real world data. The authors also suggest that it can be applied to phenomena such as natural wind-field etc.

B. B. Peng et al. [17] suggest that hardware in the loop simulation substitutes well for evaluation of vehicle suspension. Semi-active control of half vehicle suspension is evaluated using M-R (Magneto-Rheological) damper and transducers. Real-time LQG (Linear Quadratic Gaussian) control strategy is adopted in the front quarter suspension. Vertical acceleration of sprung mass for both front and rear suspension and their PSD are plotted. Also, displacement of C-grade road is provided. Acceleration response of vehicle is improved in the sensitive frequency spectrum. Hence, comfort is said to be improved.

Hans Pacejka et al. [18] analysed the tyre behaviour. He proposed a mathematical formula relating forces and moments acting on the tyre for different conditions such as longitudinal and camber slip. He proposes coefficients which define different characteristics. The formula contains physically based formulations thus avoiding the use of correction factors. Pure slip has been represented mathematically and graphically. Factors for shape and curvature of tyres are also accounted. He suggests improvements in the ‘magic formula’ by suggesting another longitudinal force characteristic.

V.Cossalter, Roberto Lot et al. [19] gave procedure of mathematical model of motorcycles and other 2 wheeled vehicles. They divide the vehicle into two functional blocks namely vehicle and steering sub-systems. Steering sub-subsystems depend on the tyre lateral force. Maneuverability and handling phenomena are studied mathematically as related to the rider torque. This provides parameters so that rider can ‘feel good’; ‘fast’ criteria can be approached objectively. Transfer function formulae for tyre are noted. They have related tyre forces and geometrical parameters of efficient maneuverability and handling aspects.

M.K. Patil et al. [20] approached the man and tractor dynamics intending to improve comfort. Tractors, military trucks and commercial vehicles are subjected to low-frequency high amplitude vibrations which cause spinal disorders. Vertical vibrations in the range 0.5 to 11 Hz can cause severe spinal problems. They recommend isolation of man from the machine using appropriate suspension. Head, torso, thorax, diaphragm, and pelvis are considered as a spring damper arrangement, attached to the chassis and the tyres; using this assumption the vibration characteristics

are analysed. On comparison of cost and vibration isolating characteristics, authors suggest tractors be provided with a seat of relaxation type.

V.Cossalter et al. [21] performed the in-plane dynamic analysis and studied the emergency braking maneuver. Behaviour of suspension under braking is studied by use of modal analysis. It is hypothesized that stopping distance could be reduced using optimal design of suspension. Motorcycle tyre lock-up is related to ratio of braking torque acting on the two wheels. The difference in braking between wet and dry conditions is also studied.

Andrea Aguggiaro et al. [22] analysed the fall of rider during racing. Dainese, the manufacturer of motorcycle racing suits, worked together with racing teams to find efficient ways of improving rider safety. Actual data was analysed from 2006 MotoGP championship. 2D data recording units were utilized for this purpose. Setup consisted of a set of 3 accelerometers and gyrometers. A GPS unit capable of recording bank angle and data logger with 400 Hz sample frequency. A low-side fall data with respect to roll, pitch and yaw is also provided. Studying the real-time racing data, they were able to understand differences between high-side and low-side on the basis of RMS value of gyrometers.

2.1 Research Objective:

- Analyse 4 dof motorcycle model for road profile. Finding out the mode shapes and the Frequency Response Function ie FRF (Verification)
- Analysing 6 dof motorcycle road for C grade profile and comparing acceleration PSD (Verification)
- Subjecting 6 dof model to realistic speed bump and finding vertical accelerations acting on the sprung mass and passenger (Problem Statement).

Chapter 3 Methodology

In plane dynamic analysis of the motorcycle is performed by representing the motorcycle as a spring-mass-damper system. For reducing complexities associated with modelling a real life system, few simplifying criteria are followed:

- The motorcycle body is divided into a system of masses, springs and dampers.
- The terminology of sprung and unsprung mass is used.
- Sprung mass by definition consists of the mass which is supported by the suspension; for example chassis, rider, handlebars, front cowl.
- The unsprung mass consists of tires, wheels, part of suspension forks and brake assembly.

For modelling the suspension system, we use the reduced stiffness and damping.

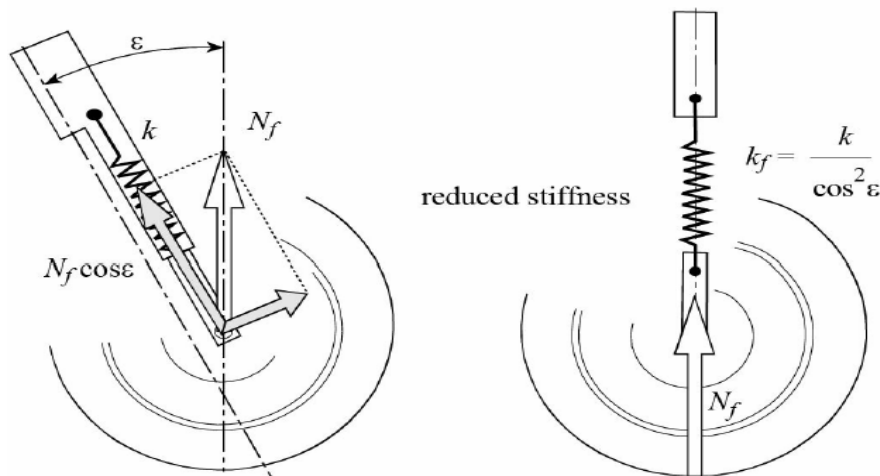


Figure 3-1: Reduced suspension for motorcycle model [2]

This approach has been used for simplifying the model [24]

Equivalence between inclined and reduced suspension:

The criteria used is that; In inclined as well as reduced suspension, the same force (N_f) should produce the same vertical displacement (x)

For the inclined suspension: $kx_{inclined} = N_f \cos \epsilon$

$$x_{inclined} = \frac{(N_f \cos \epsilon)}{k}$$

$$\frac{x_{vertical}}{\cos \epsilon} = \frac{(N_f \cos \epsilon)}{k}$$

$$x_{vertical} \text{ for inclined suspension} = \frac{(N_f \cos^2 \epsilon)}{k}$$

$$x_{vertical} \text{ for reduced suspension} = \frac{N_f}{k_f}$$

Equating $x_{vertical}$ for inclined and reduced suspensions we get,

- Reduced stiffness, $k_f = k/\cos^2 \epsilon$

Similarly if we assume damper instead of spring we find,

- Reduced Damping, $c_f = c/\cos^2 \epsilon$

Using this approach, the inclined suspension is converted to a vertical suspension.

Four DOF model is initially chosen as it is a basic model of a motorcycle

3.1: Four DOF motorcycle model

The four DOF Model consists of a sprung mass & front and rear unsprung masses.

The four DOF are: vertical displacement and rotation of the sprung mass (called bounce and pitch respectively)

Assumptions:

- The rider is assumed attached to the motorcycle i.e., there exists no relative motion between them.
- For a 4 DOF system, the sprung mass constitutes chassis, engine, rider and steering head.
- The speed of the motorcycle is assumed constant as it undergoes a straight line motion.
- The Sprung mass is represented by a rectangular homogeneous shape mass.
- No slip occurs between the tyre and the road surface

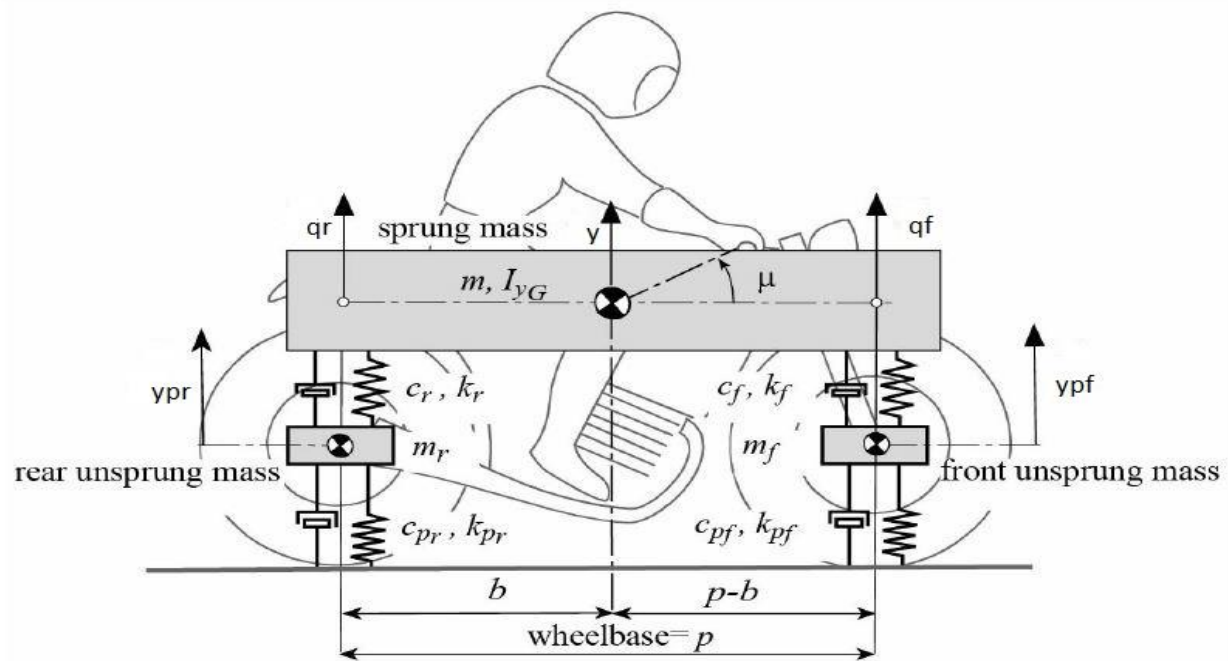


Figure 3.2: 4 DOF Motorcycle Model (Abs Co-ordinates) [24]

In figure 3.2; a 4 dof model with absolute co-ordinates is shown.

Nomenclature:

y is the vertical displacement of the sprung mass

μ is the pitching rotation of sprung mass

y_{pf} is the vertical displacement of the front unsprung mass

y_{pr} is the vertical displacement of the rear unsprung mass

c_f, k_f and c_r, k_r are damping and stiffness suspension of the front and rear suspension

c_{pf}, k_{pf} and c_{pr}, k_{pr} are damping and stiffness coefficients of the tyres

m, I_g are the mass and the pitch M.I of the sprung mass respectively

m_r, m_f are the rear and front unsprung masses respectively

p is the wheelbase

b is the distance from the C.G to the rear wheel

Data for the 4 DOF model is as follows:

Table 3.1: Motorcycle parameters for 4 DOF model adapted from [24]

Wheelbase, p (m)	1.4
Distance from the C.G to the rear wheel, b (m)	0.70
Sprung mass, m (kg)	200
Front unsprung mass, m_f (kg)	15
Rear unsprung mass, m_r (kg)	18
Pitch M.I, I_g (kg)	38
Reduced Stiffness of the front suspension, k_f (N/m)	15000
Reduced Stiffness of the rear suspension, k_r (N/m)	24000
Reduced Damping of the front suspension, c_f (Ns/m)	500
Reduced damping of the rear suspension, c_r (Ns/m)	750
Front tyre stiffness, k_{pf} (N/m)	180000
Rear tyre stiffness, k_{pr} (N/m)	180000
Front tyre damping c_{pf} (Ns/m)	0
Rear tyre damping c_{pr} (Ns/m)	0

3.1.1 Equations of motion in absolute coordinates:

From the figure 3.2, using absolute coordinates and formulating the equations of motion

$$[M]\{\ddot{y}\} + [C]\{\dot{y}\} + [K]\{y\} = 0 \quad \dots (1)$$

Where,

$$M = \begin{bmatrix} m & 0 & 0 & 0 \\ 0 & I_g & 0 & 0 \\ 0 & 0 & m_r & 0 \\ 0 & 0 & 0 & m_f \end{bmatrix}$$

$$C = \begin{bmatrix} c_f + c_r & c_f(p - b) - c_r(b) & -c_r & c_f \\ c_f(p - b) - c_r \times b & c_r \times b^2 + c_f(p - b)^2 & c_r \times b & -c_f(p - b) \\ -c_r & c_r \times b & c_r + c_{pr} & 0 \\ -c_f & -c_f(p - b) & 0 & c_f + c_{pf} \end{bmatrix}$$

$$K = \begin{bmatrix} k_f + k_r & k_f(p - b) - k_r \times b & -k_r & -k_f \\ k_f(p - b) - k_r \times b & k_r \times b^2 + k_f(p - b)^2 & k_r \times b & -k_f(p - b) \\ -k_r & k_r \times b & k_r + k_{pr} & 0 \\ -k_f & -k_f(p - b) & 0 & k_f + k_{pf} \end{bmatrix}$$

$$y = \begin{bmatrix} y \\ \mu \\ y_{pr} \\ y_{pf} \end{bmatrix}$$

Equations of motion in relative coordinates:

Using absolute coordinates we have the displacement and rotation of C.G of sprung mass. but for plotting the results, we will use the relative coordinates; so as to obtain results in the format used in [2]. Converting to relative coordinates we can find displacements for the front and rear of the sprung mass.

Converting y, μ, y_{pr}, y_{pf} (absolute) into q_r, q_f, q_{pr}, q_{pf} (relative) to analyse the sprung mass motion in a better way.

Following transformations relate the absolute & relative systems:

$$q_r = y - \mu b - y_{pr} ; \quad q_f = y + \mu a - y_{pf}$$

$$q_{pr} = y_{pr} - w_r ; \quad q_{pf} = y_{pf} - w_f ;$$

Figure 3.3 shows a schematic for converting absolute co-ordinates into relative coordinates

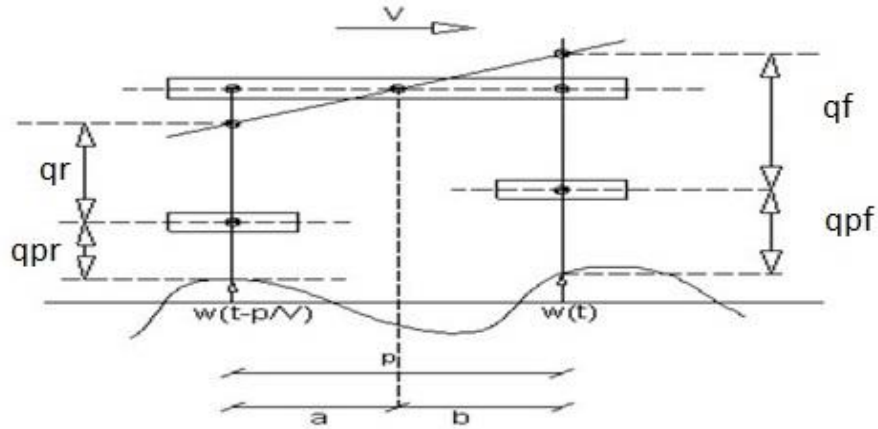


Figure 3-3: 4 DOF Motorcycle Model Relative Co-ordinates [2]

Now using equation (1) & subjecting it to road excitation at the wheels

3.1.2 Motorcycle response to road profile (frequency domain approach)

Let w is the displacement vector that excites the front & the rear wheels.

Dynamic Equilibrium for absolute coordinates is:

$$[M]\{\ddot{y}\} + [C]\{\dot{y}\} + [K]\{y\} = [\tilde{C}]\{\dot{w}\} + [\tilde{K}]\{w\} \quad \dots(2)$$

Where,

$$\tilde{C} = \begin{bmatrix} 0 & 0 & 0 & 0 \\ 0 & 0 & 0 & 0 \\ 0 & 0 & c_{pr} & 0 \\ 0 & 0 & 0 & c_{pf} \end{bmatrix}; \quad w = \begin{bmatrix} 0 \\ 0 \\ w_r \\ w_f \end{bmatrix};$$

$$\tilde{K} = \begin{bmatrix} 0 & 0 & 0 & 0 \\ 0 & 0 & 0 & 0 \\ 0 & 0 & k_{pr} & 0 \\ 0 & 0 & 0 & k_{pf} \end{bmatrix};$$

Matrices M , C , K are defined in section 3.1.1

Equation (2) is for absolute coordinates. After doing the calculations for relative coordinates for the above equation,

For relative co-ordinates

$$[\bar{M}]\{\ddot{q}\} + [\bar{C}]\{\dot{q}\} + [\bar{K}]\{q\} = -[\bar{M}]\{\ddot{w}\} \quad \dots (3)$$

Where,

$$\bar{M} = \frac{1}{p} \begin{bmatrix} am & bm & am & bm \\ -I_g & I_g & -I_g & I_g \\ 0 & 0 & p * m_r & 0 \\ 0 & 0 & 0 & p * m_f \end{bmatrix} \quad q = \begin{bmatrix} q_r \\ q_f \\ q_{pr} \\ q_{pf} \end{bmatrix}$$

$$\bar{C} = \begin{bmatrix} c_r & c_f & 0 & 0 \\ -b * c_r & a * c_f & 0 & 0 \\ -c_r & 0 & c_{pr} & 0 \\ 0 & -c_f & 0 & c_{pf} \end{bmatrix}$$

$$\bar{K} = \begin{bmatrix} k_r & k_f & 0 & 0 \\ -b * k_r & a * k_f & 0 & 0 \\ -k_r & 0 & k_{pr} & 0 \\ 0 & -k_f & 0 & k_{pf} \end{bmatrix}$$

3.1.3 Calculating the Frequency Response Function Matrix in Absolute Coordinates

Now consider equation (1)

$$[M]\{\ddot{y}\} + [c]\{\dot{y}\} + [k]\{y\} = [\tilde{C}]\{\dot{w}\} + [\tilde{K}]\{w\}$$

$$y = y_0 e^{i\omega t} \quad \dot{y} = i\omega e^{i\omega t} y_0 \quad \ddot{y} = -\omega^2 y_0 e^{i\omega t}$$

$$w = w_0 e^{i\omega t} \quad \dot{w} = i\omega e^{i\omega t} w_0 \quad \ddot{w} = -\omega^2 w_0 e^{i\omega t}$$

Substituting in Eqn (4)

$$\{y_0 e^{i\omega t}\} \{[M](-\omega^2) + [c](i\omega) + [k]\} = [i\omega \tilde{C} + \tilde{K}]\{w_0 e^{i\omega t}\}$$

$$\left\{ \frac{y_0 e^{i\omega t}}{w_0 e^{i\omega t}} \right\} = \frac{y_0}{w_0} = H_q(\omega) = [-\omega^2 M + i\omega c + k]^{-1} [i\omega \tilde{C} + \tilde{K}]$$

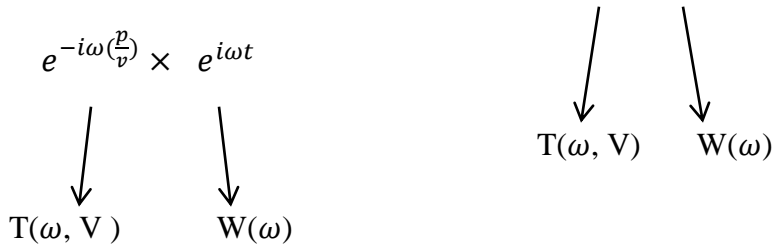
The 2 excitations to the wheel correspond to the same excitation but with a time lag of (p/V) ie wheelbase divided by velocity.

Therefore, $w = \begin{Bmatrix} 0 \\ 0 \\ w(t - \frac{p}{v}) \\ w(t) \end{Bmatrix}$

- $w = w_0 e^{i\omega(t - \frac{p}{v})}$ $w = w_0 e^{i\omega t}$

- $\frac{w}{w_0} = e^{i\omega(t - \frac{p}{v})}$ $\frac{w}{w_0} = e^{i\omega t}$

- $\frac{w}{w_0} = \frac{e^{i\omega t}}{e^{i\omega(\frac{p}{v})}}$ $\frac{w}{w_0} = 1 \times e^{i\omega t}$



- $T(\omega, v)$ is the wheel base filtering vector
- Time delay of rear wheel input relative to front one acts to filter the amplitude of vehicle motion

- $T(\omega, v) = \begin{Bmatrix} 0 \\ 0 \\ e^{-i\omega(\frac{p}{v})} \\ 1 \end{Bmatrix}$

Using this vector we can write the frf (frequency response function) in terms of ω and V

$$\widehat{H}_q(\omega, V) = [-\omega^2 M + i\omega c + k]^{-1} [i\omega \widetilde{C} + \widetilde{K}] T(\omega, V)$$

Multiplying matrices

- $\widehat{H}_q(\omega, v) = \begin{bmatrix} 0 & 0 & \widehat{H}_{y\ ypr} & \widehat{H}_{y\ ypf} \\ 0 & 0 & \widehat{H}_{\mu\ ypr} & \widehat{H}_{\mu\ ypf} \\ 0 & 0 & \widehat{H}_{ypr\ ypr} & \widehat{H}_{ypr\ ypf} \\ 0 & 0 & \widehat{H}_{ypr\ ypr} & \widehat{H}_{ypr\ ypf} \end{bmatrix} \begin{Bmatrix} 0 \\ 0 \\ e^{-i\omega(\frac{p}{v})} \\ 1 \end{Bmatrix}$

$$\bullet \widehat{H}_q(\omega, v) = \begin{bmatrix} \widehat{H}_{y ypr} e^{-i\omega(\frac{p}{v})} + \widehat{H}_{y ypf} \\ \widehat{H}_{\mu ypr} e^{-i\omega(\frac{p}{v})} + \widehat{H}_{\mu ypf} \\ \widehat{H}_{ypr ypr} e^{-i\omega(\frac{p}{v})} + \widehat{H}_{ypr ypf} \\ \widehat{H}_{ypr ypr} e^{-i\omega(\frac{p}{v})} + \widehat{H}_{ypr ypf} \end{bmatrix}$$

Following similar procedure, the matrices for relative coordinates are

$$\widehat{H}_z(\omega, v) = \begin{bmatrix} \widehat{H}_{qr qr} & \widehat{H}_{qr qf} & \widehat{H}_{qr qpr} & \widehat{H}_{qr qpf} \\ \widehat{H}_{qf qr} & \widehat{H}_{qf qf} & \widehat{H}_{qf qpr} & \widehat{H}_{qf qpf} \\ \widehat{H}_{qpr qr} & \widehat{H}_{qpr qf} & \widehat{H}_{qpr qpr} & \widehat{H}_{qpr qpf} \\ \widehat{H}_{qpf qr} & \widehat{H}_{qpf qf} & \widehat{H}_{qpf qpr} & \widehat{H}_{qpf qpf} \end{bmatrix} \begin{Bmatrix} 0 \\ 0 \\ e^{-i\omega(\frac{p}{v})} \\ 1 \end{Bmatrix}$$

$$\widehat{H}_q(\omega, v) = \begin{bmatrix} \widehat{H}_{qr qpr} e^{-i\omega(\frac{p}{v})} + \widehat{H}_{qr qpf} \\ \widehat{H}_{qf qpr} e^{-i\omega(\frac{p}{v})} + \widehat{H}_{qf qpf} \\ \widehat{H}_{qpr qpr} e^{-i\omega(\frac{p}{v})} + \widehat{H}_{qpr qpf} \\ \widehat{H}_{qpf qpr} e^{-i\omega(\frac{p}{v})} + \widehat{H}_{qpf qpf} \end{bmatrix}$$

- The relative bounce between rear end of sprung mass and rear unsprung mass is

$$\widehat{H}_{qr qpr} e^{-i\omega(\frac{p}{v})} + \widehat{H}_{qr qpf} \quad (5)$$

- The relative bounce between front end of sprung mass and front unsprung mass is

$$\widehat{H}_{qf qpr} e^{-i\omega(\frac{p}{v})} + \widehat{H}_{qf qpf} \quad (6)$$

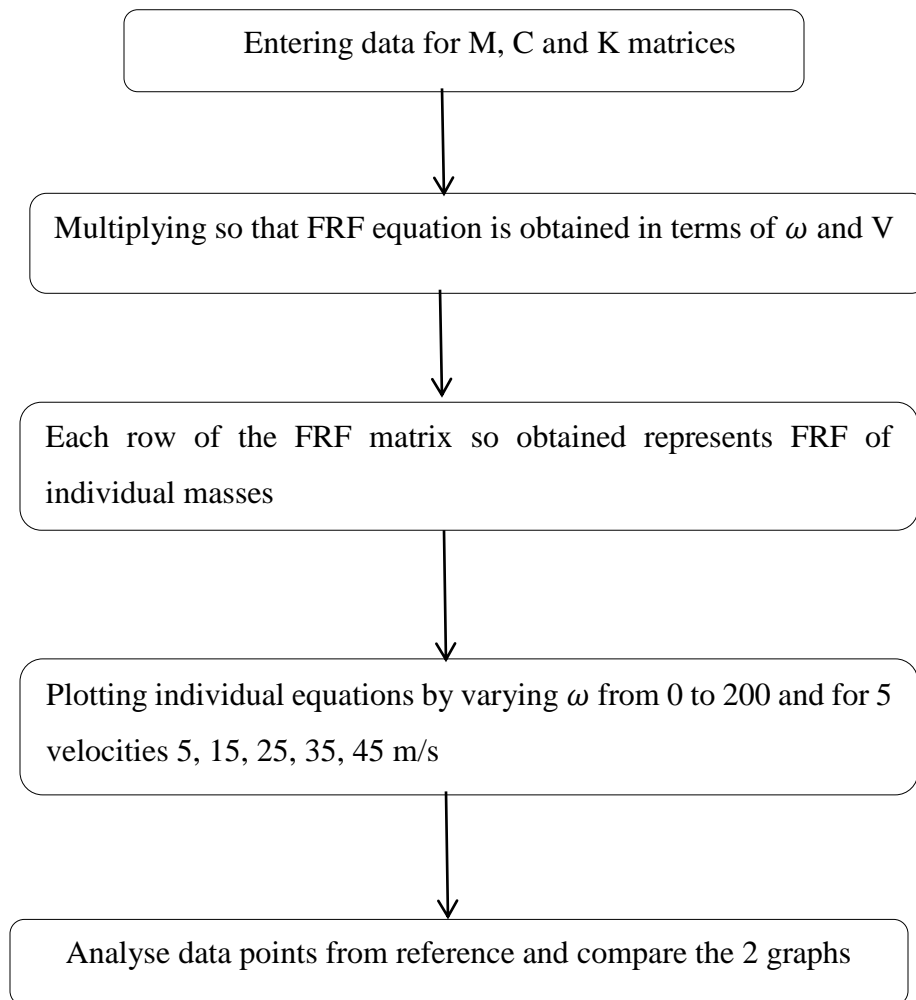
- The relative hop between rear unsprung mass and the ground is

$$\widehat{H}_{qpr qpr} e^{-i\omega(\frac{p}{v})} + \widehat{H}_{qpr qpf} \quad (7)$$

- The relative hop between front unsprung mass and the ground is

$$\widehat{H}_{qpf qpr} e^{-i\omega(\frac{p}{v})} + \widehat{H}_{qpf qpf} \quad (8)$$

Now that equations are found; The FRF are plotted using Matlab. The procedure for the same is detailed below:



Using the data in table 3.1 frf of 4 dof model is calculated.

The FRF results for 4 DOF model are plotted in Result section 4.1

3.2: Six DOF motorcycle model

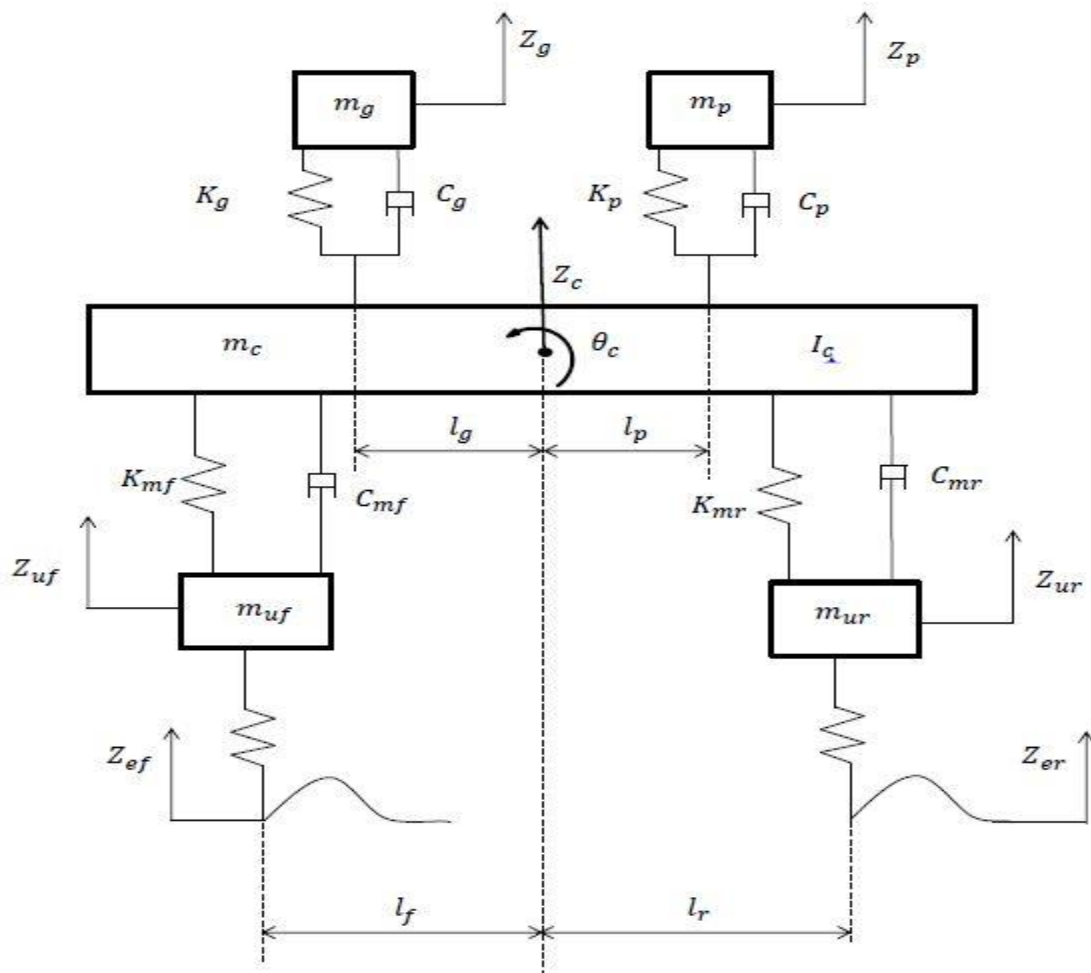


Figure 3.4: 6 DOF Motorcycle Model

$m_g, m_p, m_c, m_{uf}, m_{ur}$ represent the masses of engine, rider, motorcycle body (sprung mass), front and rear unsprung mass respectively

k_{mf}, c_{mf} and k_{mr}, c_{mr} are the stiffness and damping coefficient of the front and rear suspension respectively

k_{uf} and k_{ur} are the tire stiffness of front and rear tires respectively.

k_g and c_g are the stiffness and damping coefficient of engine

k_p and c_p are the stiffness and damping coefficient of passenger

l_f, l_r, l_g, l_p are the distances from the front axle, rear axle, engine and driver to the sprung mass centre respectively.

The equations of motion for the above system under road excitation are:

$$\begin{aligned}
& \dot{z}_c(m_c) + z_c(k_{mf} + k_{mr} + k_g + k_p) + \theta_c(-k_{mf}l_f + k_{mr}l_r + k_g l_p - k_p l_p) \\
& + z_{uf}(-k_{mf}) + z_{ur}(-k_{mr}) + z_g(-k_g) + z_p(-k_p) \\
& + \dot{z}_c(c_{mf} + c_{mr} + c_g + c_p) + \dot{\theta}_c(-c_{mf}l_f + c_{mr}l_r + c_g l_p - c_p l_p) \\
& + \dot{z}_{uf}(-c_{mf}) + \dot{z}_{ur}(-c_{mr}) + \dot{z}_g(-c_g) + \dot{z}_p(-c_p) = 0
\end{aligned} \tag{A}$$

$$\begin{aligned}
& \ddot{\theta}_c(I_c) + z_c(-k_{mf}l_f + k_{mr}l_r - k_g l_p + k_p l_p) + \theta_c(k_{mf}l_f^2 + k_{mr}l_r^2 - k_g l_p^2 - k_p l_p^2) \\
& + z_{uf}(k_{mf}l_f) + z_{ur}(-k_{mr}l_r) + z_g(k_g l_p) - z_p(k_p l_p) \\
& + \dot{z}_c(-c_{mf}l_f + c_{mr}l_r - c_g l_p + c_p l_p) + \\
& \dot{\theta}_c(c_{mf}l_f^2 + c_{mr}l_r^2 - c_g l_p^2 - c_p l_p^2) + \dot{z}_{uf}(c_{mf}l_f) + \\
& \dot{z}_{ur}(-c_{mr}l_r) + \dot{z}_g(c_g l_p) - \dot{z}_p(c_p l_p) = 0
\end{aligned} \tag{B}$$

$$\begin{aligned}
& \ddot{z}_{uf}(m_{uf}) - z_c(k_{mf}) + \theta_c(k_{mf}l_f) + z_{uf}(k_{mf}) + z_{uf}(k_{uf}) \\
& - \dot{z}_c(c_{mf}) + \dot{\theta}_c(c_{mf}l_f) + \dot{z}_{uf}(c_{mf}) = k_{uf}z_{ef}
\end{aligned} \tag{C}$$

$$\begin{aligned}
& \ddot{z}_{ur}(m_{ur}) - z_c(k_{mr}) - \theta_c(k_{mr}l_r) + z_{ur}(k_{mr}) + z_{ur}(k_{ur}) \\
& - \dot{z}_c(c_{mr}) - \dot{\theta}_c(c_{mr}l_r) + \dot{z}_{ur}(c_{mr}) = k_{ur}z_{er}
\end{aligned} \tag{D}$$

$$\begin{aligned}
& \ddot{z}_g(m_g) - z_c(k_g) - \theta_c(k_g l_p) + z_g(k_g) \\
& + \dot{z}_c(c_g) - \dot{\theta}_c(c_p l_p) + \dot{z}_p(c_p) = 0
\end{aligned} \tag{E}$$

$$\ddot{z}_p(m_p) - z_c(k_p) + \theta_c(k_p l_p) + z_p(k_p) + \dot{z}_c(c_p) - \dot{\theta}_c(c_p l_p) + \dot{z}_p(c_p) = 0 \tag{F}$$

These equations of motion are 2nd order differential equation. It is far more convenient to solve first order differential equations rather than conventional second order differential equations in MATLAB which brings us to state space form

3.2.1 State space form:

A state space representation is a mathematical model of a physical system as a set of input, output and state variables, connected to each other by first order differential equations. If the dynamic system is linear, time-invariant and finite dimensional, then the differential and algebraic equations may be written in the matrix form.

State space representation is also known as the ‘time domain’ approach. It provides an efficient manner to model and analyse system with multiple input and outputs

Assuming there are ‘n’ second order differential equations, we can change them to ‘2n’ first order equations. This form of writing equations of motion in first order is called as state space form.

Steps for converting the equations of motion into state space form:

1. Firstly write the equations in their usual form of $M\ddot{z} + c\dot{z} + kz = F$

Rewrite the equation so that LHS becomes \ddot{z} that is move the stiffness and damping terms on the opposite side and divide them by the mass matrix(or multiply by inverse of mass matrix.)

2. Change the notation to another variable say in this case X.

Say $X_1 = z_1$ Position of mass 1

and $X_2 = \dot{z}_1$ Velocity of mass 1 and so on

3. Rewrite the equations now in terms of X1, X2, X3 and so on.

Now, the form of equations would be

$$\dot{X}_1 = [-(\text{stiffness and damping terms})/m] X_1 + [F_1/m_1]$$

$$\dot{X}_2 = [-(\text{stiffness and damping terms})/m] X_2 + [F_2/m_2]$$

4. After combining we get, $\dot{X}_n = AX + BU$, U in this case is an input variable

B is the input matrix, the nature changes based on the input used.

The number of outputs changes depending on whether the system is a SISO (Single Input Single Output) or a MIMO (Multiple Input Multiple Output).

In our analysis of six dof model we have used state space formulation. The 6 DOF motorcycle model is of type MIMO as it has 2 inputs viz bump at the front and rear tyre. Thus the no. of columns of system and input matrices are changed accordingly which are detailed in the further sections.

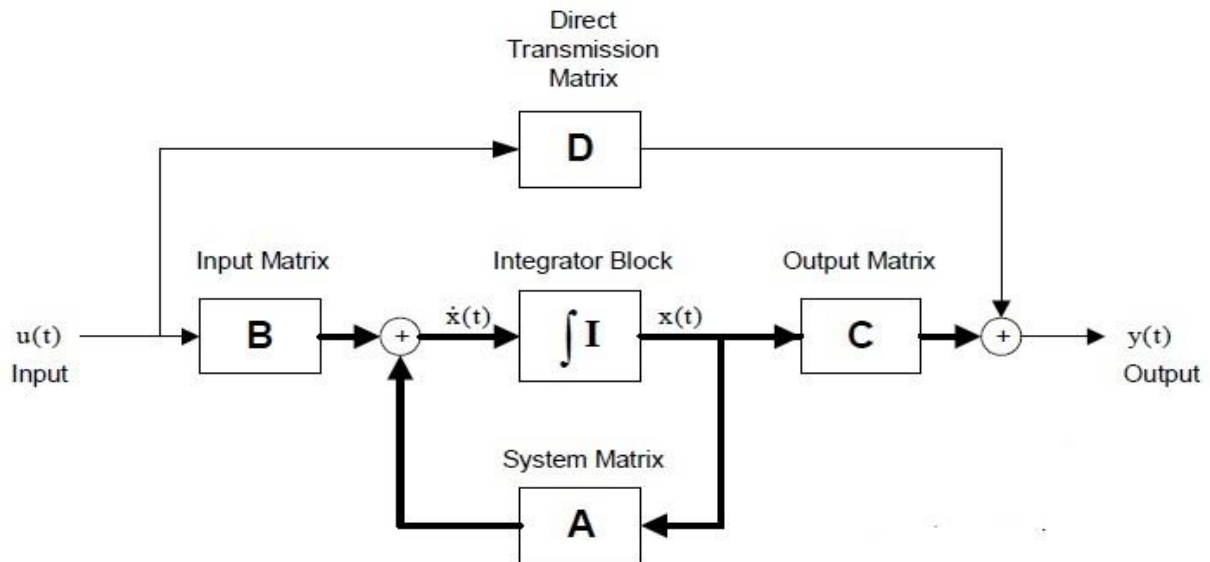


Figure 3.5: State space block explanation [25]

Output Matrix:

- Output Matrix C is used, when desired output is not restricted to the states, but is rather a combination of the input states (In this thesis, both front and rear tyre have different inputs at different times)

Output formulation $y = CX + DU$

- The matrix D is called as the direct transmission matrix. It is used for some special cases. It is primarily used to include in output some inputs that sidestep the normal states as shown in figure 3-6.

For the output matrix,

No of rows of output matrix C = no. of output required

No of columns of output matrix C=no of system states

As seen in the figure 3.5, A and B matrices are passed through the integral block.

In 6 DOF motorcycle model, D is assumed zero.

3.2.2 State space formulation of the 6 dof model:

Consider equation (A),

- Taking the stiffness and damping terms to the RHS and dividing by mass:

$$\ddot{z}_c = \frac{1}{m_c} \{ -[c_{mf} + c_{mr} + c_g + c_p] \dot{z}_c - [-c_{mf}l_f + c_{mr}l_r + c_gl_g - c_pl_p] \dot{\theta}_c \\ + c_{mf} \dot{z}_{uf} + c_{mr} \dot{z}_{ur} + c_g \dot{z}_g + c_p \dot{z}_p - [k_{mf} + k_{mr} + k_g + k_p] z_c \\ - [-k_{mf}l_f + k_{mr}l_r + k_gl_p - k_pl_p] \theta_c + k_{mf} z_{uf} + k_{mr} z_{ur} \\ + k_g z_g + k_p z_p \}$$

- Converting to state space so as to convert system to first order differential equation

Selecting state vector $X = [z_c \ \dot{z}_c \ \theta_c \ \dot{\theta}_c \ z_{uf} \ \dot{z}_{uf} \ z_{ur} \ \dot{z}_{ur} \ z_g \ \dot{z}_g \ z_p \ \dot{z}_p]$;

$X = [X_1 \ X_2 \ X_3 \ X_4 \ X_5 \ X_6 \ X_7 \ X_8 \ X_9 \ X_{10} \ X_{11} \ X_{12}]$;

- From above,

$$\dot{X}_1 = X_2 \\ \dot{X}_2 = \frac{1}{m_c} \{ -[c_{mf} + c_{mr} + c_g + c_p] X_2 - [-c_{mf}l_f + c_{mr}l_r + c_gl_g - c_pl_p] X_4 \\ + c_{mf} X_6 + c_{mr} X_8 + c_g X_{10} + c_p X_{12} - [k_{mf} + k_{mr} + k_g + k_p] X_1 \\ - [-k_{mf}l_f + k_{mr}l_r + k_gl_p - k_pl_p] X_3 + k_{mf} X_5 + k_{mr} X_7 \\ + k_g X_9 + k_p X_{11} \}$$

Employing similar procedure for remaining equations B to F;

We arrive at a standard form,

$\dot{X} = AX + BU$ which is the state space formulation.

$Y = CX + DU$ which is the output formulation

A is the system matrix; B is the input matrix.

C is the output matrix (sprung mass and rider output) and D is direct transmission matrix.

The state space matrices are as follows:

A=

$$\begin{bmatrix}
 0 & 1 & 0 & 0 & 0 & 0 & 0 & 0 & 0 & 0 & 0 & 0 \\
 (k_{mf} & (c_{mf} & (k_{mf}l_f & (c_{mf}l_f & & & & & & & & \\
 +k_{mr} & +c_{mr} & -k_{mr}l_r & -c_{mr}l_r & & & & & & & & \\
 +k_g & +c_g & -k_g l_g & -c_g l_g & & & & & & & & \\
 +k_p) & +c_p) & +k_p l_p) & +c_p l_p) & \frac{k_{mf}}{m_c} & \frac{c_{mf}}{m_c} & \frac{k_{mr}}{m_c} & \frac{c_{mr}}{m_c} & \frac{k_g}{m_c} & \frac{c_g}{m_c} & \frac{k_p}{m_c} & \frac{c_p}{m_c} \\
 -\frac{m_c}{m_c} & -\frac{m_c}{m_c} & -\frac{m_c}{m_c} & -\frac{m_c}{m_c} & 0 & 0 & 0 & 0 & 0 & 0 & 0 & 0 \\
 0 & 0 & 0 & 1 & 0 & 0 & 0 & 0 & 0 & 0 & 0 & 0 \\
 (k_{mf}l_f & (c_{mf}l_f & (k_g l_g^2 & (c_g l_g^2 & & & & & & & & \\
 -k_{mr}l_r & -c_{mr}l_r & +k_p l_p^2 & +c_p l_p^2 & & & & & & & & \\
 +k_g l_g & +c_g l_g & -k_{mf}l_f^2 & -c_{mf}l_f^2 & & & & & & & & \\
 -k_p l_p) & -c_p l_p) & -k_{mr}l_r^2) & -c_{mr}l_r^2) & -\frac{k_{mf}l_f}{I_c} & -\frac{c_{mf}l_f}{I_c} & \frac{k_{mr}l_r}{I_c} & \frac{c_{mr}l_r}{I_c} & -\frac{k_g l_g}{I_c} & -\frac{c_g l_g}{I_c} & \frac{k_p l_p}{I_c} & \frac{c_p l_p}{I_c} \\
 \frac{I_c}{I_c} & \frac{I_c}{I_c} & \frac{I_c}{I_c} & \frac{I_c}{I_c} & 0 & 1 & 0 & 0 & 0 & 0 & 0 & 0 \\
 0 & 0 & 0 & 0 & 0 & 0 & 0 & 0 & 0 & 0 & 0 & 0 \\
 \frac{k_{mf}}{m_{uf}} & \frac{c_{mf}}{m_{uf}} & -\frac{k_{mf}l_f}{m_{uf}} & -\frac{c_{mf}l_f}{m_{uf}} & -\frac{(k_{mf} & -\frac{c_{mf}}{m_{uf}} & 0 & 0 & 0 & 0 & 0 & 0 \\
 +k_{uf})}{m_{uf}} & -\frac{c_{mf}}{m_{uf}} & 0 & 0 & 0 & 0 & 0 & 0 & 0 & 0 & 0 & 0 \\
 0 & 0 & 0 & 0 & 0 & 0 & 0 & 1 & 0 & 0 & 0 & 0 \\
 \frac{k_{mr}}{m_{ur}} & \frac{c_{mr}}{m_{ur}} & \frac{k_{mr}l_r}{m_{ur}} & \frac{c_{mr}l_r}{m_{ur}} & 0 & 0 & -\frac{(k_{mr} & -\frac{c_{mr}}{m_{ur}} & 0 & 0 & 0 & 0 \\
 +k_{ur})}{m_{ur}} & -\frac{c_{mr}}{m_{ur}} & 0 & 0 & 0 & 0 & 0 & 0 & 0 & 0 & 0 & 0 \\
 0 & 0 & 0 & 0 & 0 & 0 & 0 & 0 & 0 & 1 & 0 & 0 \\
 \frac{k_g}{m_g} & \frac{c_g}{m_g} & \frac{k_p l_p}{m_g} & \frac{c_p l_p}{m_g} & 0 & 0 & 0 & 0 & -\frac{k_g}{m_g} & -\frac{c_g}{m_g} & 0 & 0 \\
 \frac{m_g}{m_g} & \frac{m_g}{m_g} & \frac{m_g}{m_g} & \frac{m_g}{m_g} & 0 & 0 & 0 & 0 & 0 & 0 & 0 & 0 \\
 0 & 0 & 0 & 0 & 0 & 0 & 0 & 0 & 0 & 0 & 0 & 1 \\
 \frac{k_p}{m_p} & \frac{c_p}{m_p} & -\frac{k_p l_p}{m_p} & -\frac{c_p l_p}{m_p} & 0 & 0 & 0 & 0 & 0 & 0 & -\frac{k_p}{m_p} & -\frac{c_p}{m_p} \\
 \frac{m_p}{m_p} & \frac{m_p}{m_p} & -\frac{m_p}{m_p} & -\frac{m_p}{m_p} & 0 & 0 & 0 & 0 & 0 & 0 & \frac{m_p}{m_p} & \frac{m_p}{m_p}
 \end{bmatrix}$$

Matrix A which is the system matrix is a 12×12 matrix.

The system parameters of stiffness and damping are incorporated in matrix A

Thus, Matrix A represents the system in state space form

B=

$$\begin{bmatrix} 0 & 0 \\ 0 & 0 \\ 0 & 0 \\ 0 & 0 \\ 0 & 0 \\ \frac{k_{uf}}{m_{uf}} & 0 \\ 0 & 0 \\ 0 & \frac{k_{ur}}{m_{ur}} \\ 0 & 0 \\ 0 & 0 \\ 0 & 0 \\ 0 & 0 \end{bmatrix}$$

The B Matrix has two columns as there are two inputs into the system. The first column is for the front wheel input and the second column is for the rear wheel input.

C=

$$\begin{bmatrix} \begin{pmatrix} k_{mf} \\ +k_{mr} \\ +k_g \\ +k_p \end{pmatrix} & \begin{pmatrix} c_{mf} \\ +c_{mr} \\ +c_g \\ +c_p \end{pmatrix} & \begin{pmatrix} k_{mf}l_f \\ -k_{mr}l_r \\ -k_gl_g \\ +k_pl_p \end{pmatrix} & \begin{pmatrix} k_{mf}l_f \\ -k_{mr}l_r \\ -k_gl_g \\ +k_pl_p \end{pmatrix} & \frac{k_{mf}}{m_c} & \frac{c_{mf}}{m_c} & \frac{k_{mr}}{m_c} & \frac{c_{mr}}{m_c} & \frac{k_g}{m_c} & \frac{c_g}{m_c} & \frac{k_p}{m_c} & \frac{c_p}{m_c} \\ -\frac{k_p}{m_p} & -\frac{c_p}{m_p} & -\frac{-k_pl_p}{m_p} & -\frac{-c_pl_p}{m_p} & 0 & 0 & 0 & 0 & 0 & 0 & -\frac{k_p}{m_p} & -\frac{c_p}{m_p} \end{bmatrix}$$

The C Matrix contains the terms from the second and the twelfth row of the system matrix as they represent the sprung mass and the passenger. This ensures the output represents the response of the sprung mass and passenger.

D, direct transmission matrix= [0]

Table 3.2 parameters for 6 DOF motorcycle model [4]

Passenger mass m_p [kg]	80
Reduced Stiffness of the passenger k_p [N/m]	1800
Reduced Damping of the passenger c_p [N.s/m]	250
Mass of the Engine m_g [kg]	15
Stiffness of the engine k_g [N/m]	20000
Damping of the engine c_g [N.s/m]	760
Sprung mass m_c [kg]	50
Pitch Moment of Inertia I_c [kg]	80
Front unsprung mass m_{uf} [kg]	25
Rear unsprung mass m_{ur} [kg]	25
Front suspension stiffness k_{mf} [N/m]	7600
Rear suspension stiffness k_{mr} [N/m]	40000
Front suspension damping c_{mf} [N.s/m]	750
Rear suspension damping c_{mr} [N.s/m]	2000
Front tyre stiffness k_{uf} [N/m]	180000
Rear tyre stiffness k_{ur} [N/m]	220000
Distance of front axle from C.G l_f [m]	0.58
Distance of rear axle from C.G l_r [m]	0.88
Distance of passenger from C.G l_p [m]	0.3
Distance of engine from C.G l_g [m]	0.1
Speed V [km/h]	80

Substituting the values of parameters for establishing the state space A, B, C, D matrices, we proceed to make the model in Simulink. But first we generate the c grade road profile inputs for the front and rear wheels.

3.2.3 Generating C grade Road profile for front wheel

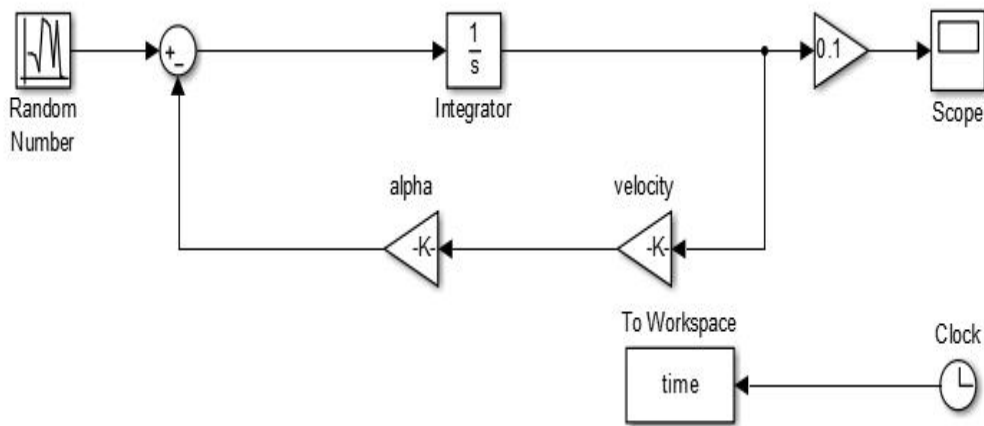


Fig 3.6: Generating Input for the front tyre

From [4], similar method is adopted for generating C grade road random input

Model Explanation:

The Random Number block generates normally distributed random numbers. The sequence so obtained is repeatable provided the block has the same non-repeatable parameters. The block outputs a signal of the same dimensionality of the parameters used. The default time-step used is 0.1 which matches the default sample time-step of a white noise block with limited bandwidth.

The velocity V is m/s and the parameter α whose value is 0.127 is input along the random block input into the integrator.

The timer block measures time and saves it to the workspace as a variable 'time'.

Following this procedure, the time curve for the front wheel is generated.

3.2.4 Generating C grade road profile for rear wheel

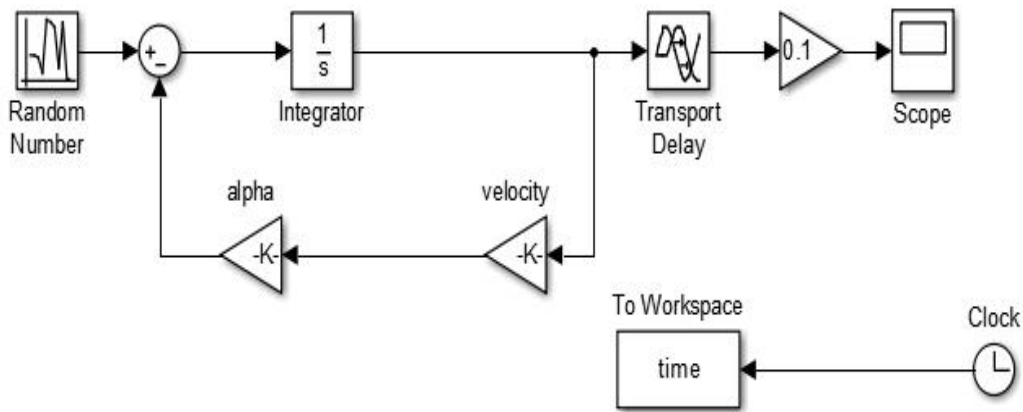


Fig 3.7: Generating Input for the rear tyre

The Transport Delay block defers the input by a pre-determined time interval, thus incorporating a time delay in the model.

However, this block should have a signal of continuous nature. During the simulation the block stores input and simulation data as a buffer till the delay ends.

The time delay is given by wheelbase divided by velocity

$$I_e = (l_f + l_r) / V = 1.46 / 22.22 = 0.065 \text{ sec}$$

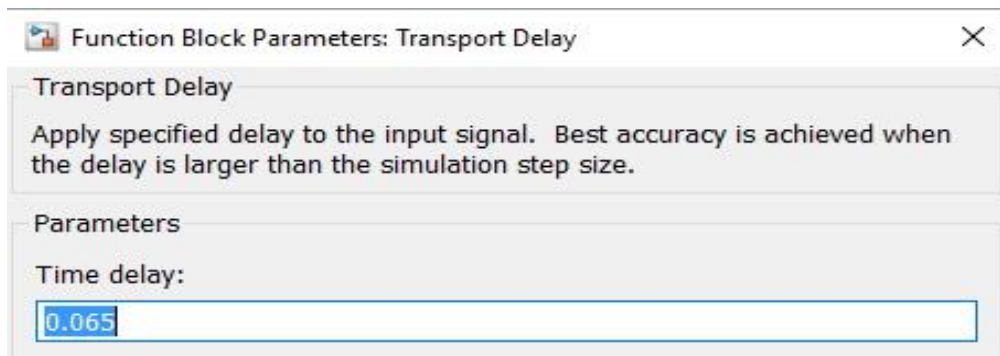


Fig 3.8: Lag values in the transport delay block

The results for 6 dof verification of c-grade road are in section 4.2

3.2.5 6 DOF model for C grade road in Simulink (for verification)

Establishing the state space model for the six DOF in Simulink

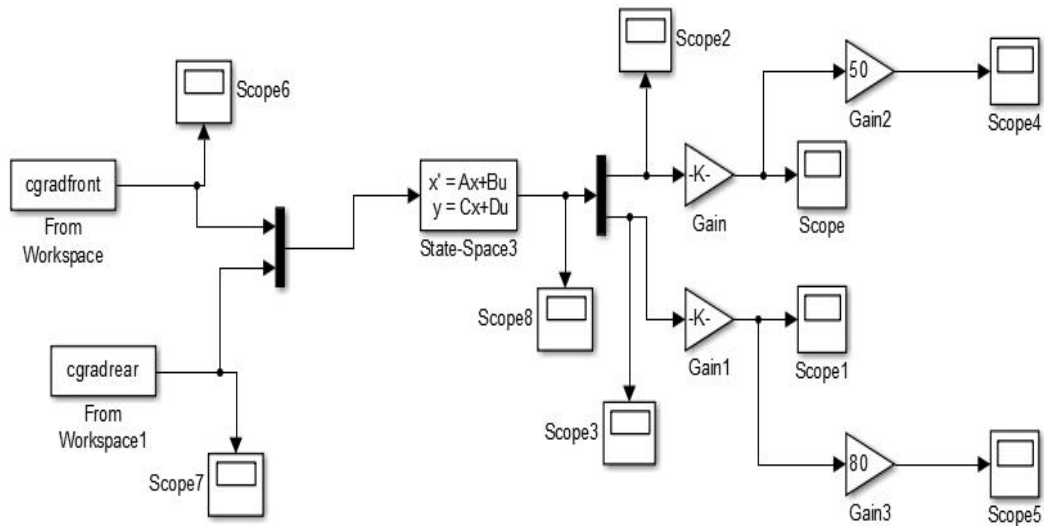


Figure 3.9: Simulink Model for 6 DOF motorcycle (C grade road)

The Simin 'from workspace' block is used to import data from the Matlab workspace.

In the above model, the cgradfront and cgradrear are the simin blocks used to import matrices representing the front wheel and rear wheel input. This input is imported from Matlab workspace. The front and rear inputs for C grade road are also generated using Simulink and have been explained in the previous sections 3.2.3 and 3.2.4.

The 'Mux' block combines its input into a single output, but it retains the individuality. All inputs must be of same data type and have an equal number of time-steps.

The state space block implements a system whose behaviour is defined as

$$\dot{x} = Ax + Bu$$

$$y = Cx + Du$$

x is the state vector and y represents the output.

The numeric values of A, B, C, D are entered in the block as follows:

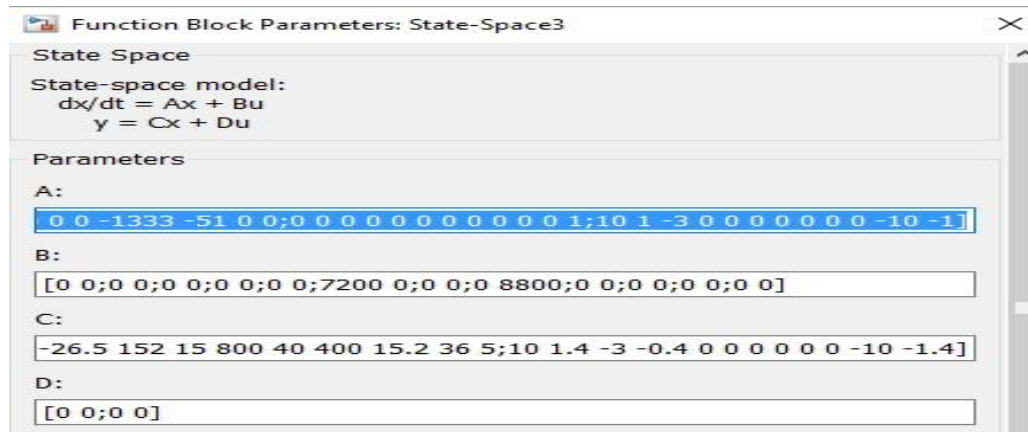


Figure 3.10: Entering A, B, C, D values in the state space block

The 'Demux' block extracts the component of an input signal and outputs the component as separate signals. It basically splits the combined signal into required outputs.

The 'Gain' block multiplies the input by a constant value (gain). In the above model, the gain block is used to multiply mass so as to find force spectrum.

The Simulink 'Scope' block displays time domain signals with respect to simulation time. The scope block is used to verify that the input is of the desired nature and is present at each stage of output operations.

3.3 Realizing realistic bump in a 6 DOF Model (Problem Statement):

Steps for generating 6 DOF response to a speed bump:

1. Generating the input for the system.
2. First plotting height vs width plot of the speed breaker.
3. Using velocity and wheelbase data to convert into height vs time.

Thus, the speed breaker data is converted into time domain which is pre requisite for using LSIM (linear simulation) tool.

4. Putting the two channel inputs into Matlab LSIM.
5. Obtaining results.

Generating Input for the system:

- The data for the speed bump has been obtained from the Portland Bureau of Transportation (PBOT) site. The figure for the same has been established on the next page
- Plotting height vs width plot of the speed bump:
- Dividing the speed bump into 3 zones
Zone 1: 1st parabola;
Zone 2: Straight region;
Zone 3: 2nd parabola
- Now, Formulating the data points and using them to design the equations for the three zones
- Equations of zone 1: $y(i) = -0.035 * x(i)^2 + 1.033 * x(i)$
Equations of zone 2: $y(i) = 7.5 + 0 * x(i)$
Equations of zone 3: $y(i) = -0.0355 * x(i)^2 + 2.877 * x(i) - 50.729$

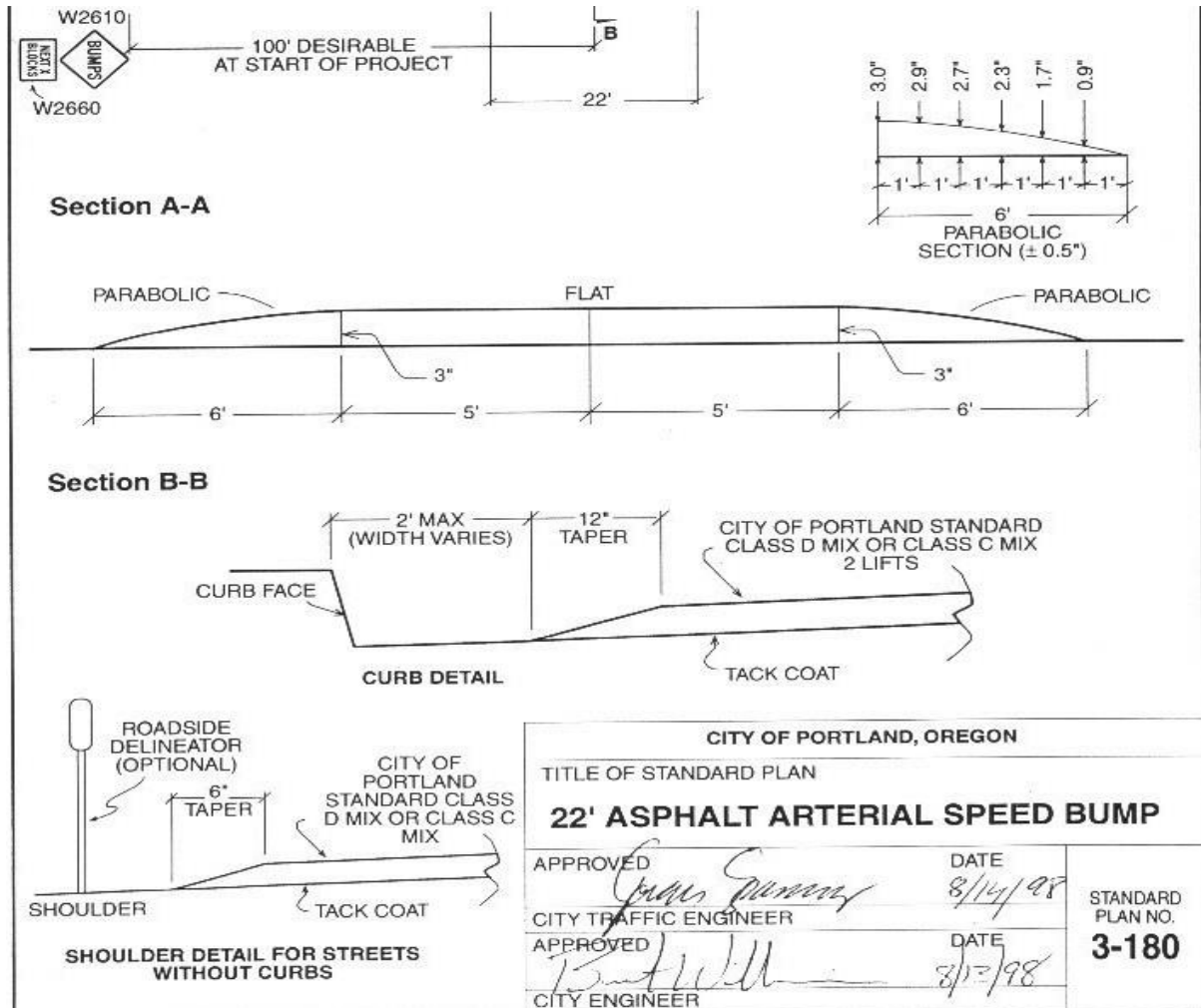


Figure 3.11: Design Data for speed bump [23]

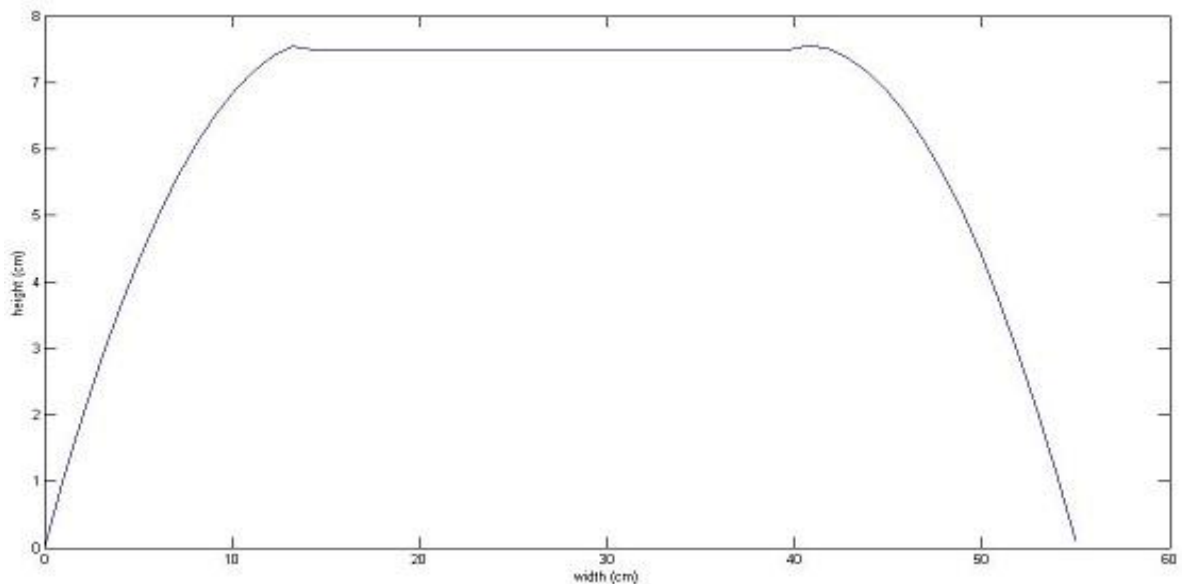


Figure 3.12: height vs width plot in Matlab

Converting the plot into Time domain:

- The three zones are divided into 1000 time steps
- Speed of the motorcycle passing over the speed bump is assumed 10 km/h=2.77 m/s

Wheelbase=1.46m

Assuming that as the vehicle moves forward both of its wheels pass over the same speed bump.

Therefore time lag between the wheels for the same speed bump

$$=1.46/2.22=0.525 \text{ sec}$$

- Dividing the distances by the motorcycle forward velocity and thus converting it into time domain.
- Following the same steps as before to formulate equations of regions and plot the speed bump profile

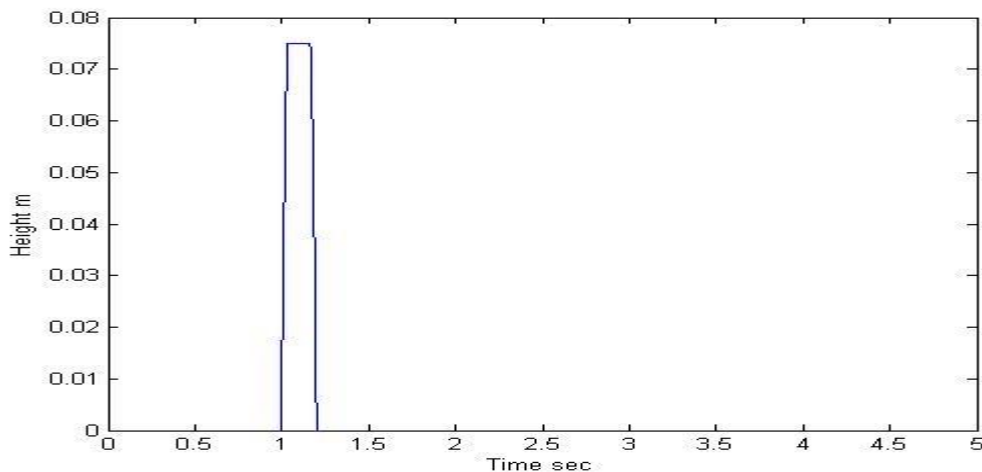


Figure 3.13: Realistic bump for front wheel

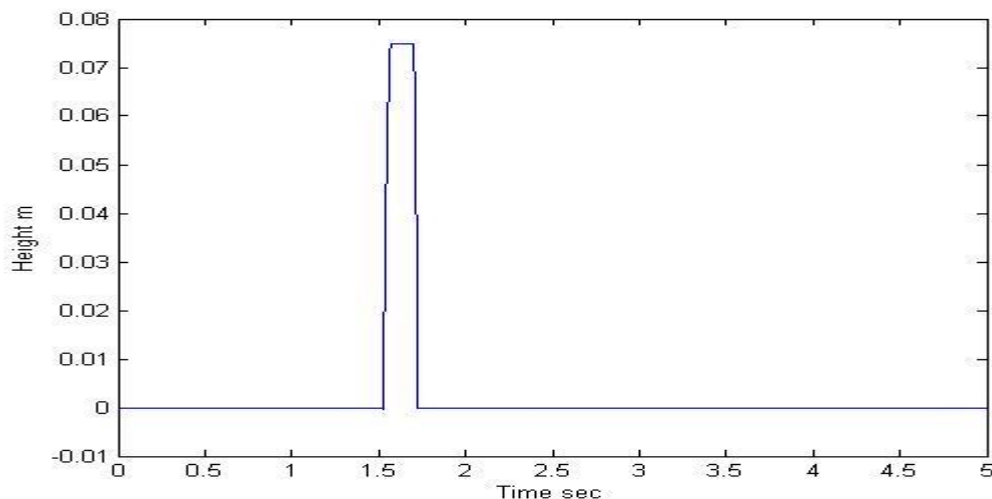


Figure 3.14: Realistic bump for rear wheel

Linear Simulation Tool:

Lsim (sys) invokes the Linear System Analyzer tool.

The linear simulation tool can be used for simulating linear models as well as state space models.

The applications of linear Simulation tool are as follows:

- It can import arbitrary input signals from the workspace.
- It can import signals from MAT file, Excel Spreadsheet or other such formats such as ASCII flat file.
- Generate pre-defined inputs such as sine wave, square, step function

Invoking the LSIM tool:

Typing `sys=ss(A,B,C,D)` in the Matlab command window. The system reads sys as a state space matrix and assigns vector X1 to X12.

Now typing `lsim(sys)` leads to:

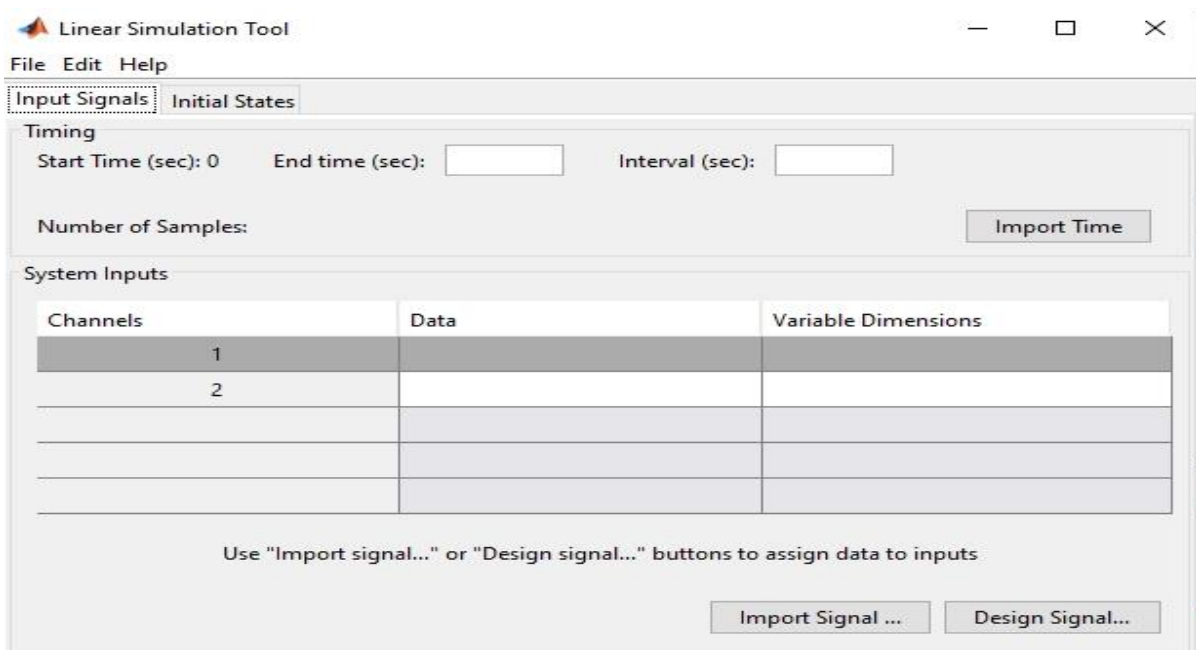


Figure 3.15: Linear Simulation Tool

Specifying the simulation time in the timing area and putting interval of 0.001 sec the following step shows the process to import data:

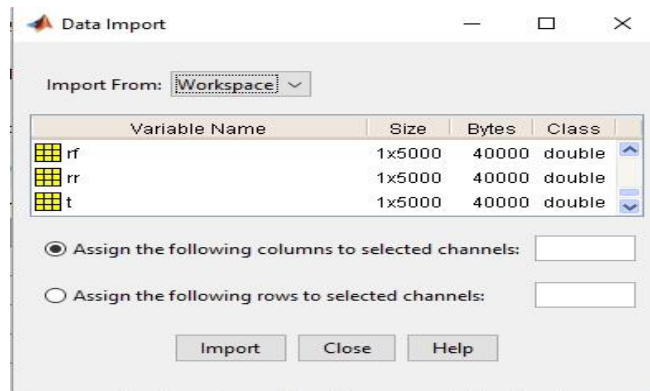


Figure 3.16: Procedure for data import

Limitation of lsim:

Lsim does not allow further analysis of output. This is where more of Simulink blocks are utilized in this thesis

LTIVIEW (sys): It stands for linear time invariant view. LTIVIEW enables to find many responses and plots such as response to step and impulse inputs and plots such as Nyquist plot, Nichols plot, Bode plot, Bode magnitude plot. It can also perform same linear simulation as lsim. It can be said that lsim is a subset of Ltiview. The different plots of ltiview are obtained by clicking plot configurations.

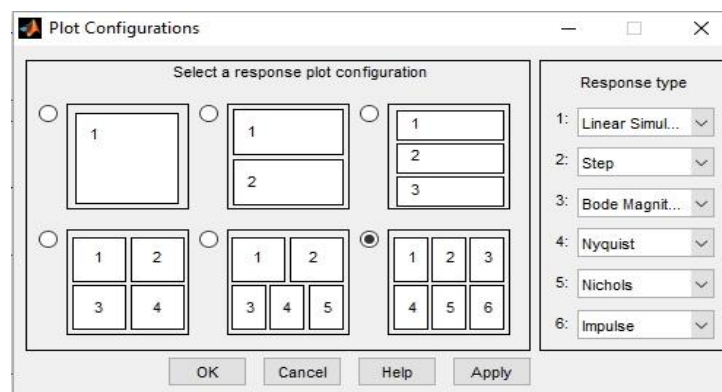


Figure 3.17: Plot configurations of LTI View

Using $sys1=tf(sys)$ we can find the transfer function of the system $damp(sys)$ displays a table of the damping ratio, natural frequency of the model (state space model sys).

3.3.1 6 DOF model for realistic bump in Simulink

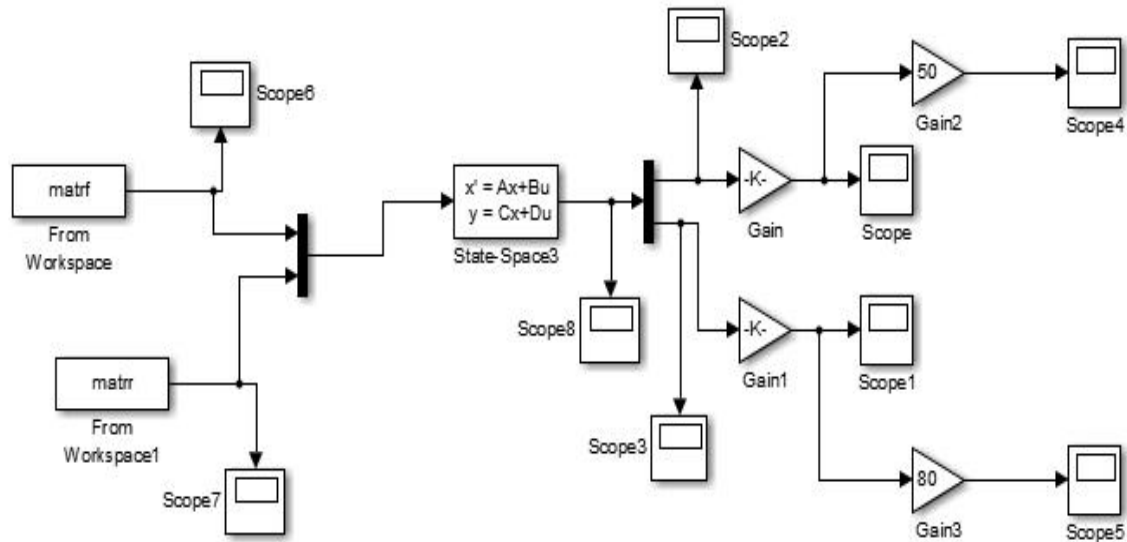


Figure 3.18: Simulink Model for 6 DOF motorcycle (Realistic bump)

Two separate Matlab programs are written for the realistic bump input, one for the front and other for the rear wheel

matrf (figure 3.13) and matrr (figure 3.14) are front and rear speed bump profiles which serve as input to the Simulink model.

This input is imported from the Matlab workspace into the Simulink model shown in figure 3.18

The gain block is multiplied by mass and thus force spectrum is obtained from the acceleration spectrum.

The results for realistic bump are in result section 4.3

3.4: 6 DOF system for triangular bump (For comparison with 5 DOF PSD)

From reference [3], the results for a 5 DOF subjected to a triangular bump are reported.

Since the data for 5 DOF motorcycle model is unavailable, the triangular bump is simulated on the 6 DOF Model for which we have the data available from [4].

Dimensions (in mm) for the so said triangular bump are:

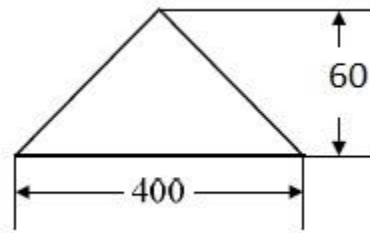


Figure 3.19: Triangle bump [3]

Representing the triangular bump in Matlab

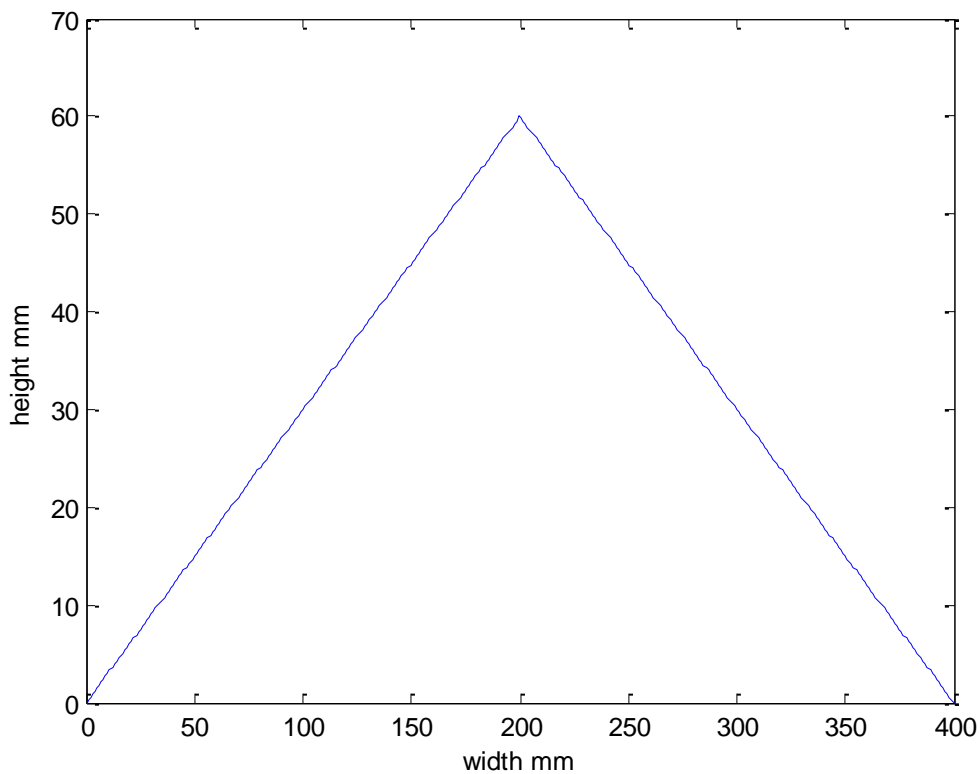


Figure 3.20: Triangle bump from MATLAB

Following similar procedure and plotting the input for front and rear tyre for $v=30$ km/h since the values are plotted for range 10 to 60 km/h. The time lag is $p/V = 1.46/8.33=0.1752$ sec.

The triangular bump for the front and rear wheels are plotted below:

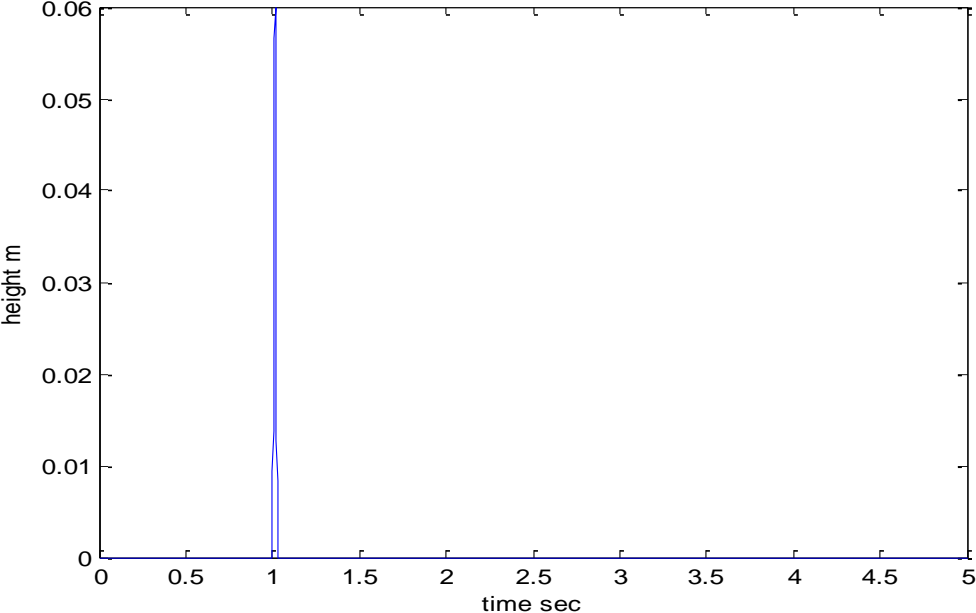


Figure 3.21: Triangular bump for front wheel

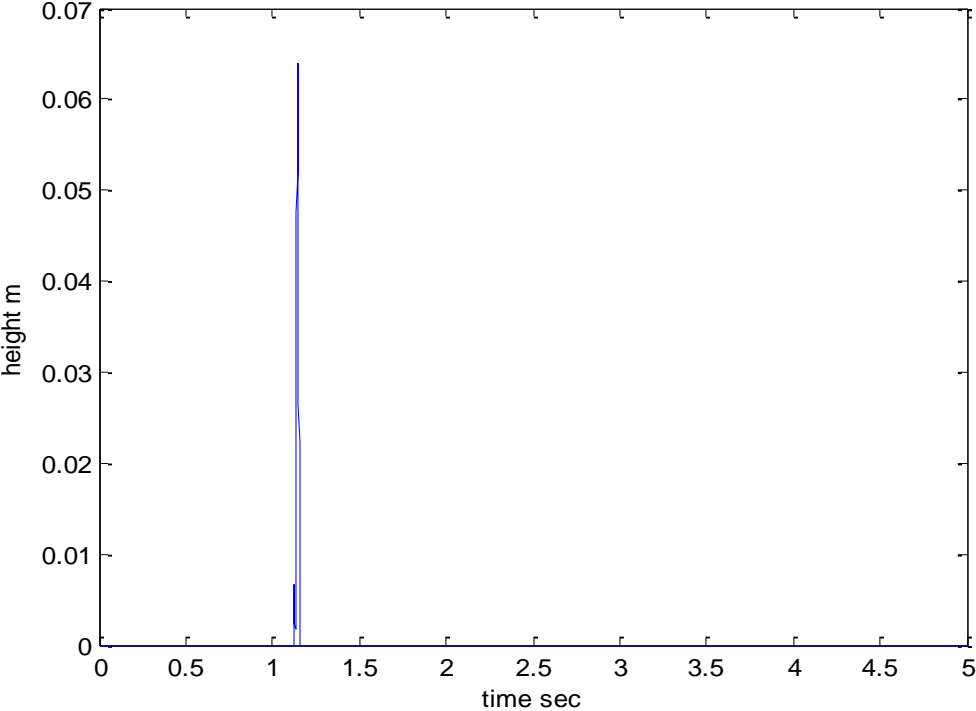


Figure 3.22: Triangular bump for rear wheel

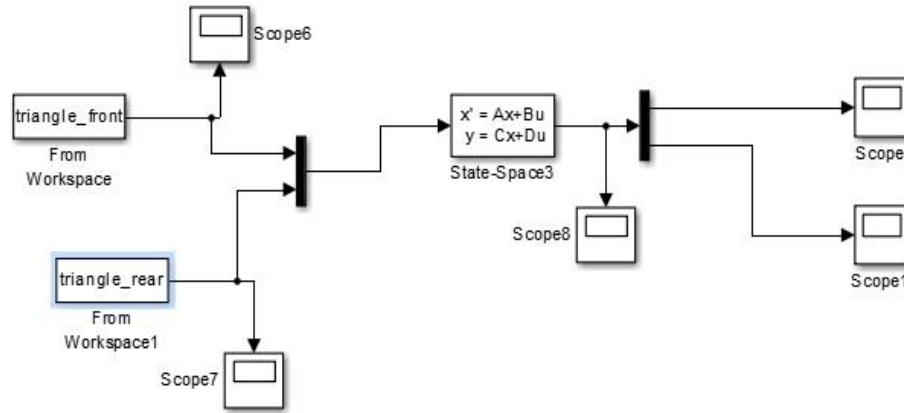


Figure 3.23: Simulink Model for triangular bump

Explanation of the Model:

- The triangle_front and the triangle_rear represent the inputs imported from the Matlab workspace into Simulink.
- The velocity of the motorcycle is assumed to be 50 km/hr. This velocity is used for plotting the input curves.

Calculation of acceleration PSD:

- In this case, the displacement response is obtained in the scope.
- The procedure from [2] is followed to convert displacement response to acceleration PSD
- Firstly the displacement response is subjected to FFT and PSD algorithm.
- The algorithm for one sided PSD is followed with the NFFT (No. of Fourier Transform Points) value of 1024.
- The data is obtained from the plot..
- Using Grabit Matlab program, the data is extracted from the 50 km/h vertical passenger acceleration; and is plotted against the PSD above obtained.

The results for the triangular bump are plotted in result section 4.4

Chapter 4: Results and Discussion

4.1: Four DOF Model Verification (Computation of the frequency response function plots):

Using the data from table [3.1] and the equation (5,6,7,8), the FRF for 4 DOF model are calculated for motorcycle speed of 25 m/s.

The computed Natural Frequency using Matlab are:

- rear bounce of sprung mass, $q_r = 21.47$ rad/s
- front bounce of sprung mass, $q_f = 12.7629$ rad/s
- Front hop (front unsprung mass), $q_{pf} = 106.7038$ rad/s
- Rear hop (rear unsprung mass), $q_{pr} = 114.110$ rad/s.

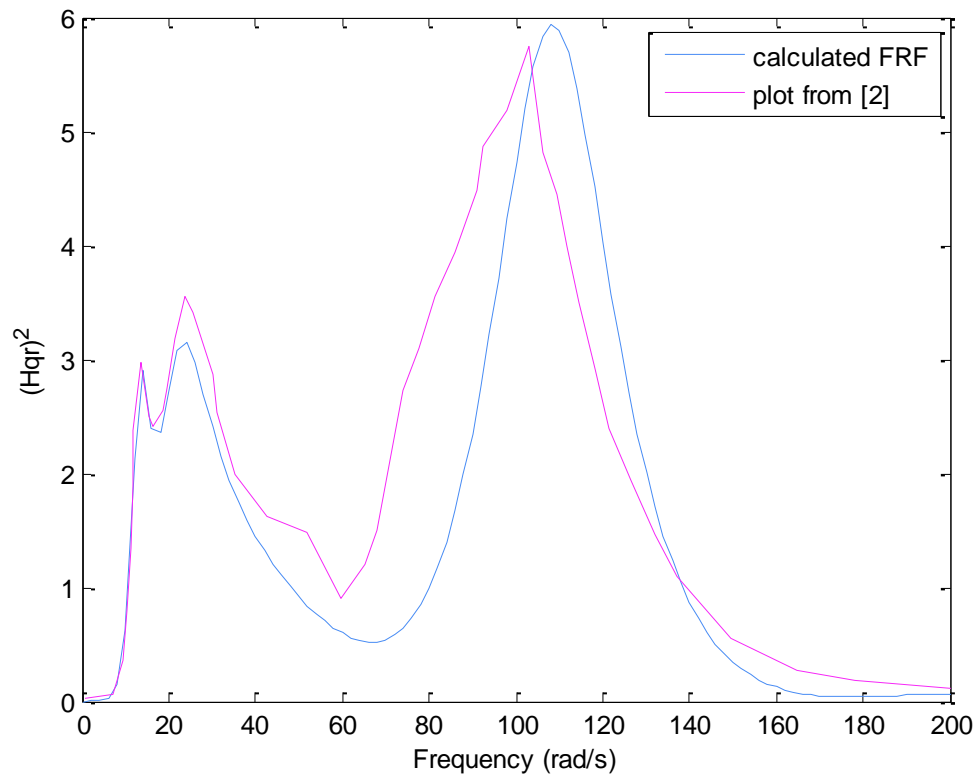


Figure 4.1: Frequency Response for rear sprung mass

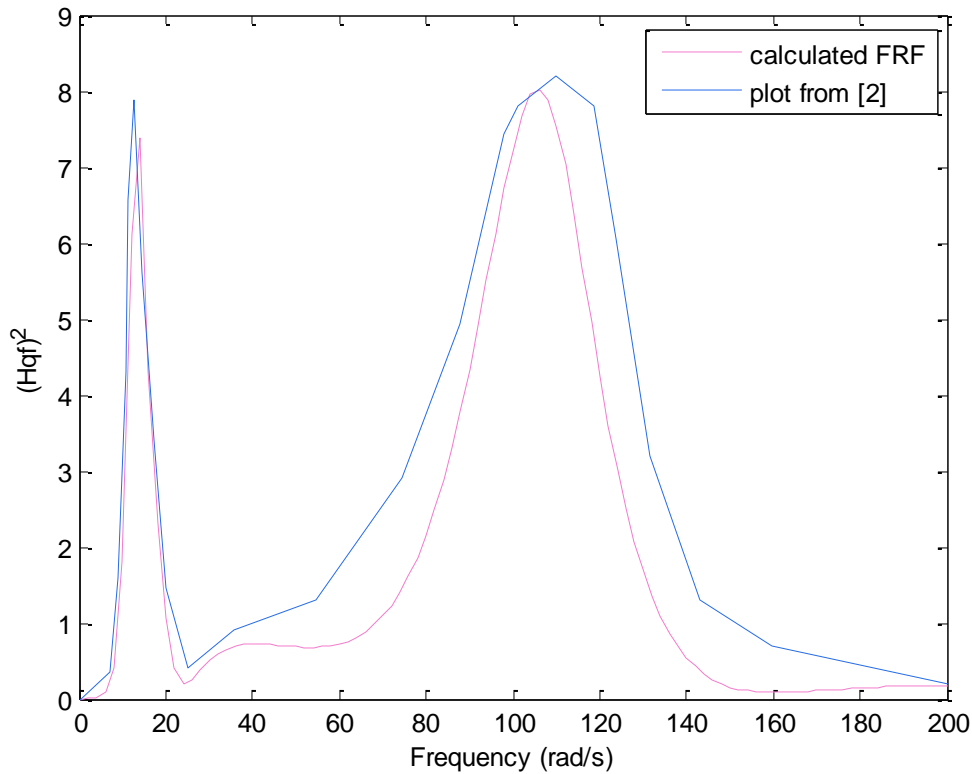


Figure 4.2: Frequency Response of front sprung mass

From Figure 4.1, It is observed that for lower frequencies, the rise in amplitude is very sudden and rapid until it reaches first maximum near front bounce frequency (12.76 rad/s) of sprung mass.

Also the second peak is reached near the rear bounce frequency (21.47 rad/s) of sprung mass. Third peak is obtained at 110 rad/s which lies between the front and rear hop frequencies of 106 and 114 rad/s.

From Figure 4.2, as is the case with 4.1, the rise in amplitude is very sudden and steep. The first peak occurs at 12.76 rad/s which agrees with front bounce frequency of sprung mass.

The second peak occurs at 110 rad/s which lies between the respective front and rear hop frequencies of 106 and 114 rad/s.

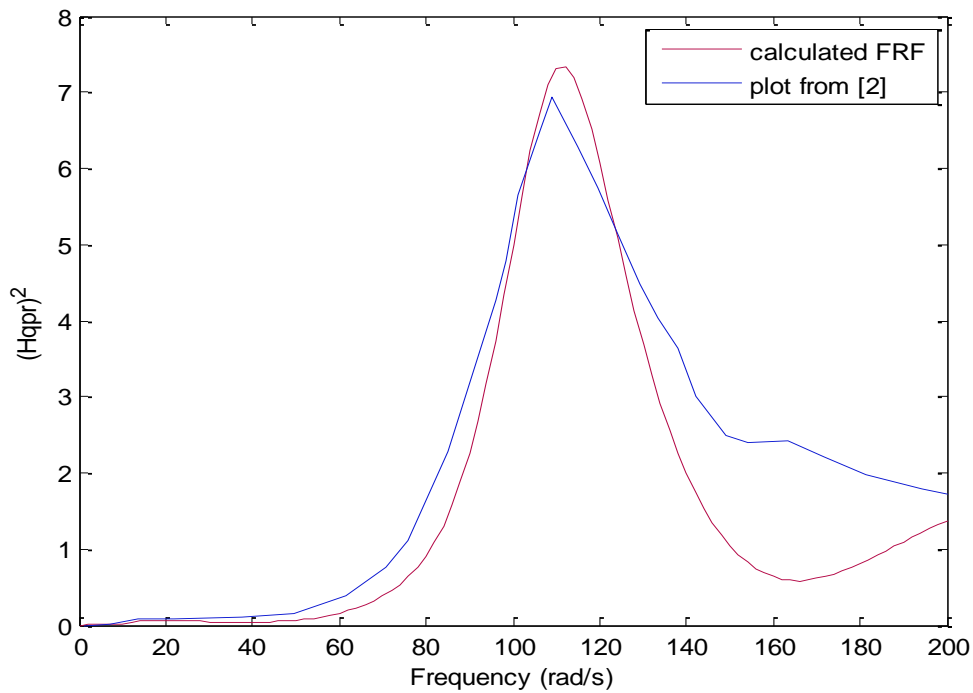


Figure 4.3: Frequency response function of rear unsprung mass

Figure 4.3 for rear unsprung mass and Fig 4.4 for front unsprung mass show a constant behaviour for various speeds. A strong presence of rear hop mode occurs at approx. 106 rad/s and front hop occurs at 114 rad/s. The maxima for the modes are evident in both the plots.

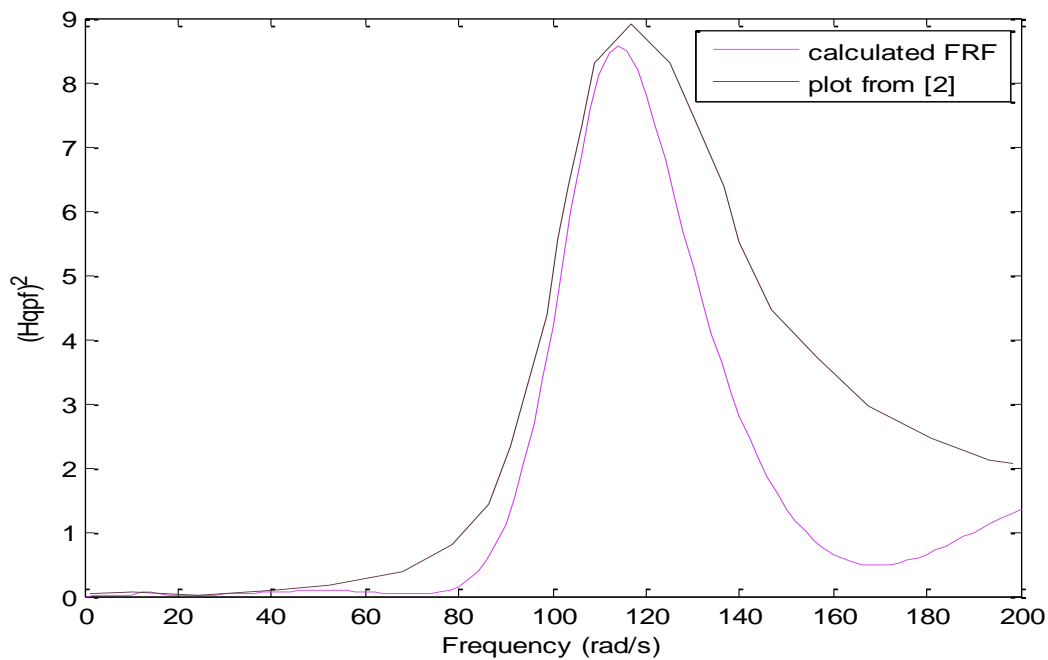


Figure 4.4: Frequency response function of front unsprung mass

4.2: 6 DOF Model Results for C grade road (verification):

The random profile of the road has been found using the random number block from Simulink whereas from the reference [4], they have utilised the harmony super-position method.

First Matlab and Simulink results are plotted followed by reference paper results.

Input for the front wheel(displacement in m vs time in s):

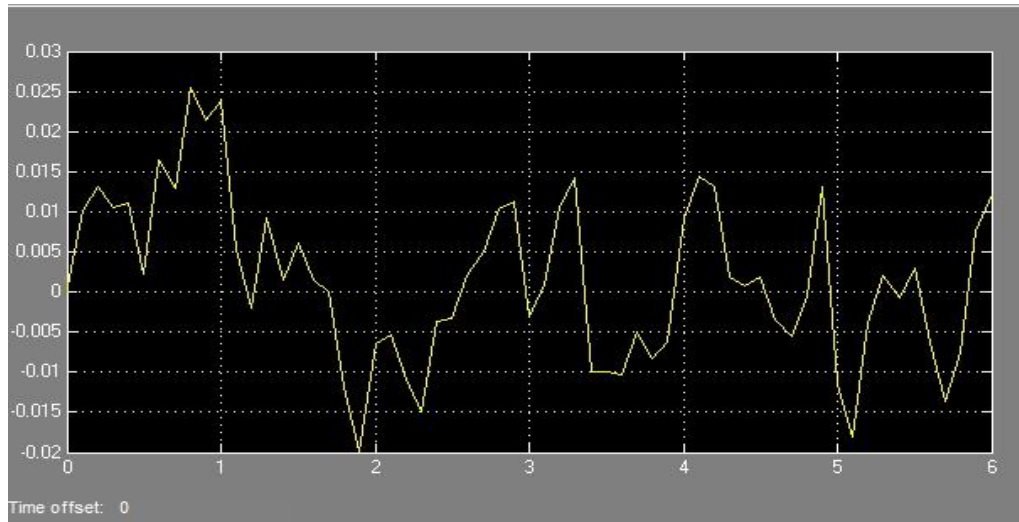


Figure 4.5: Front wheel input obtained from Simulink

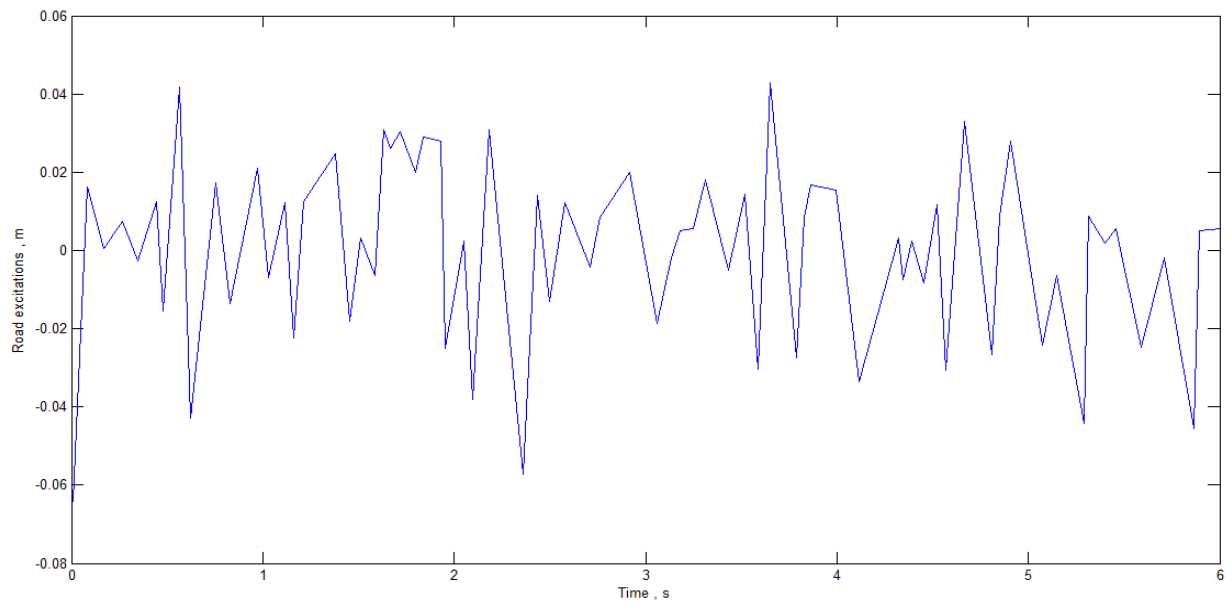


Figure 4.6: Front wheel input [4]

The slight difference in the graphs is due to difference of methods used and also due to the nature of random vibrations.

Input for the rear wheel(displacement,m vs time,s):

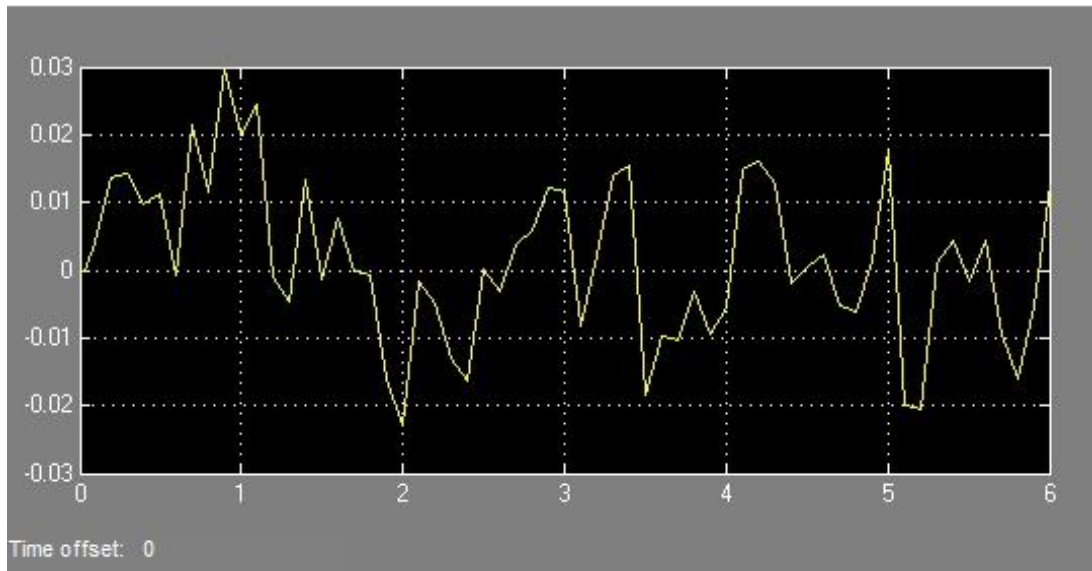


Figure 4.7: Rear wheel input obtained from Simulink

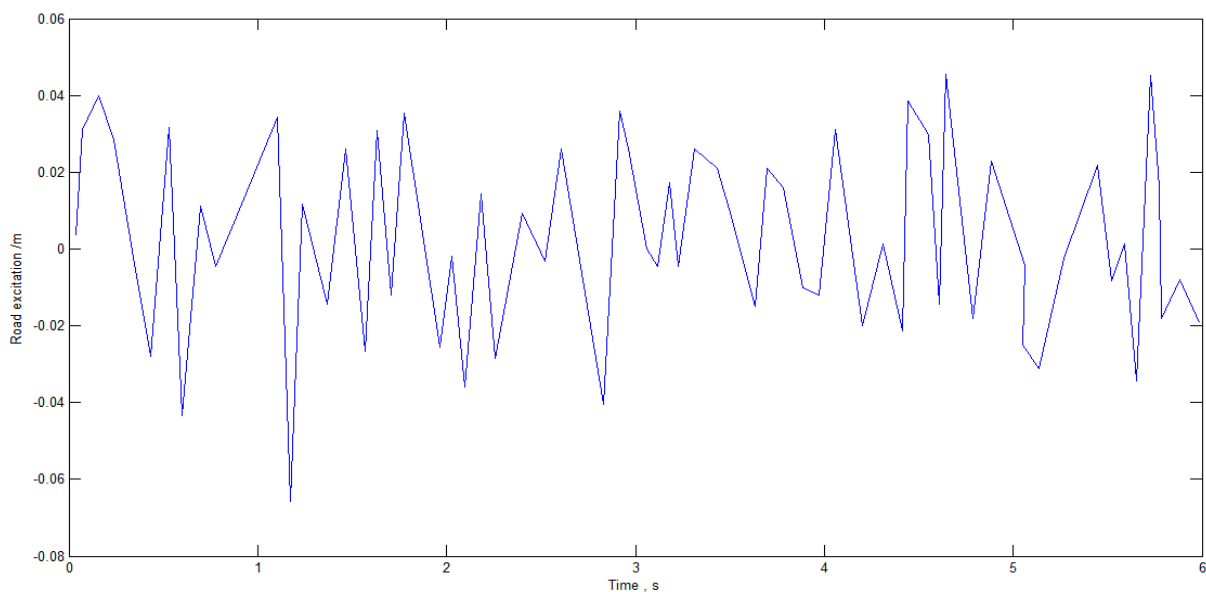


Figure 4.8: Rear wheel input [4]

The slight offset in the starting point of the graph is the time lag. In simulink, Transport Delay block has been used for providing lag to random signal.

Vertical Accelerations of the sprung mass:

Acceleration (m/s^2) vs time (sec)

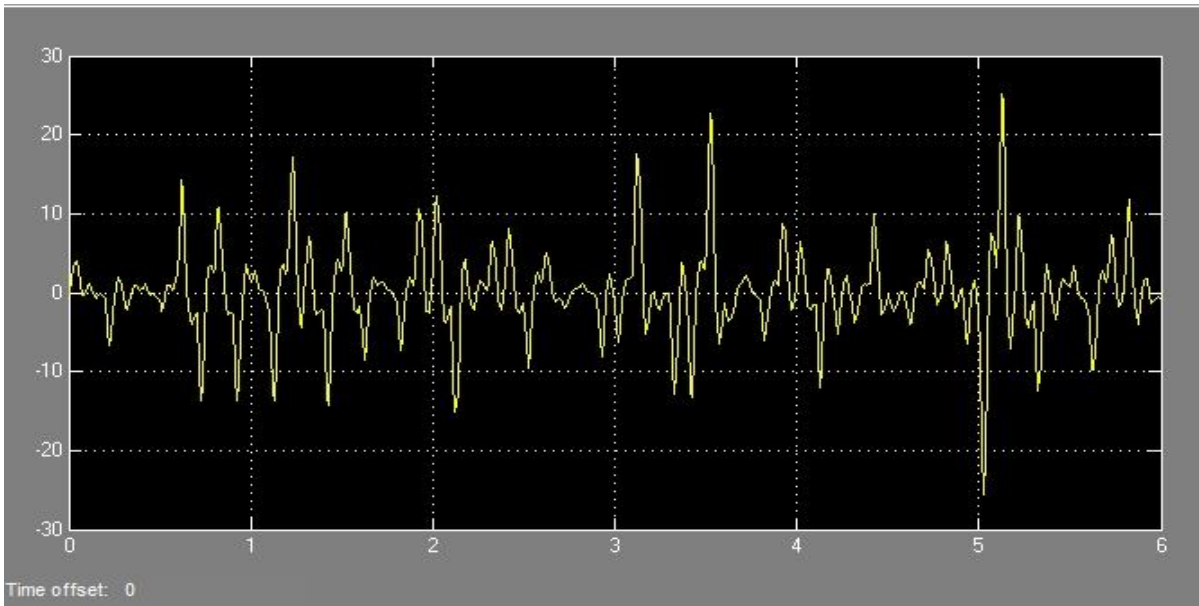


Figure 4.9: Vertical Acceleration of Sprung mass (Simulink Scope)

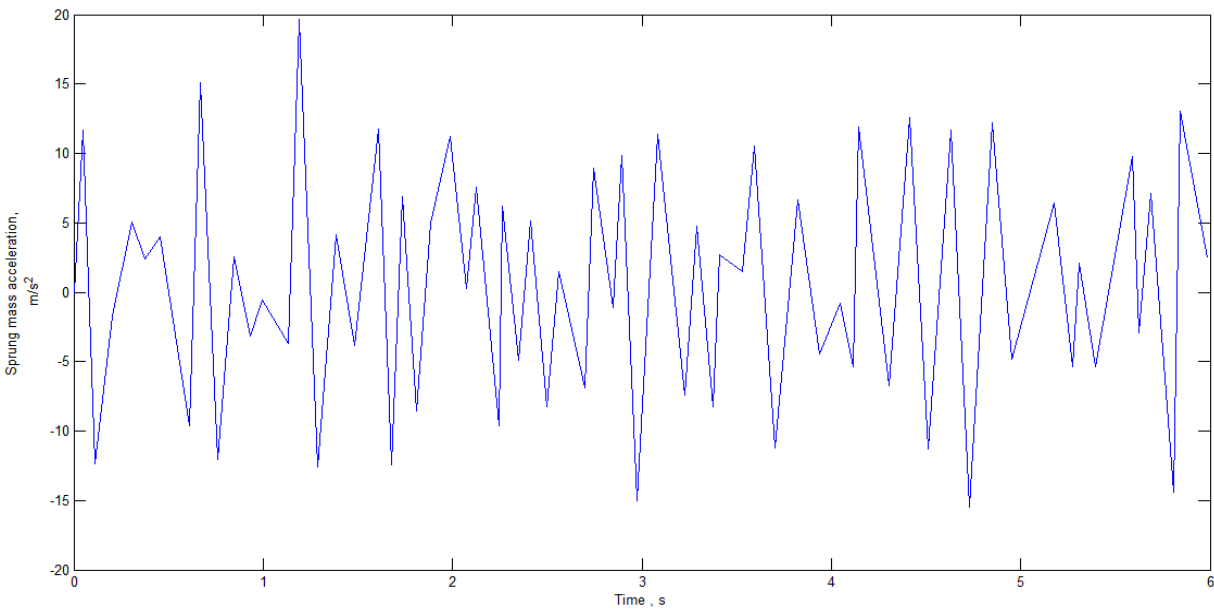


Figure 4.10: Vertical Acceleration of sprung mass [4]

The maximum acceleration obtained by simulink is around 25 m/s^2 and from the reference is around 20 m/s^2 . If we compare results for both graphs in 1 sec interval, they are similar in nature.

Vertical Acceleration of the passenger:

Acceleration (m/s^2) vs time (sec)

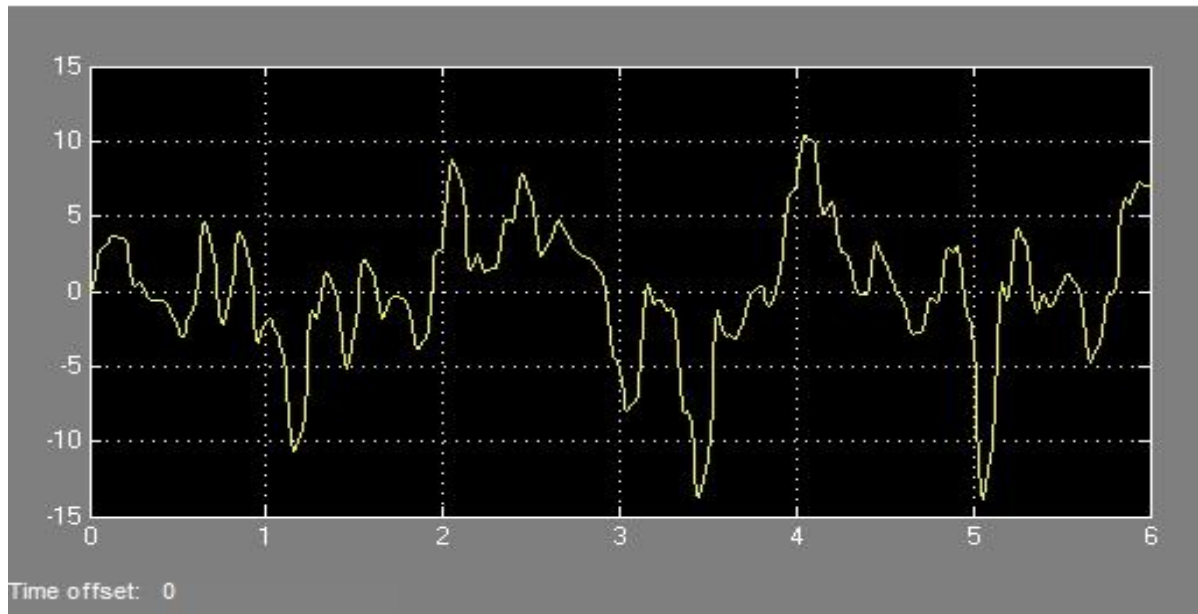


Figure 4.11: Vertical Acceleration of Passenger (Simulink Scope)

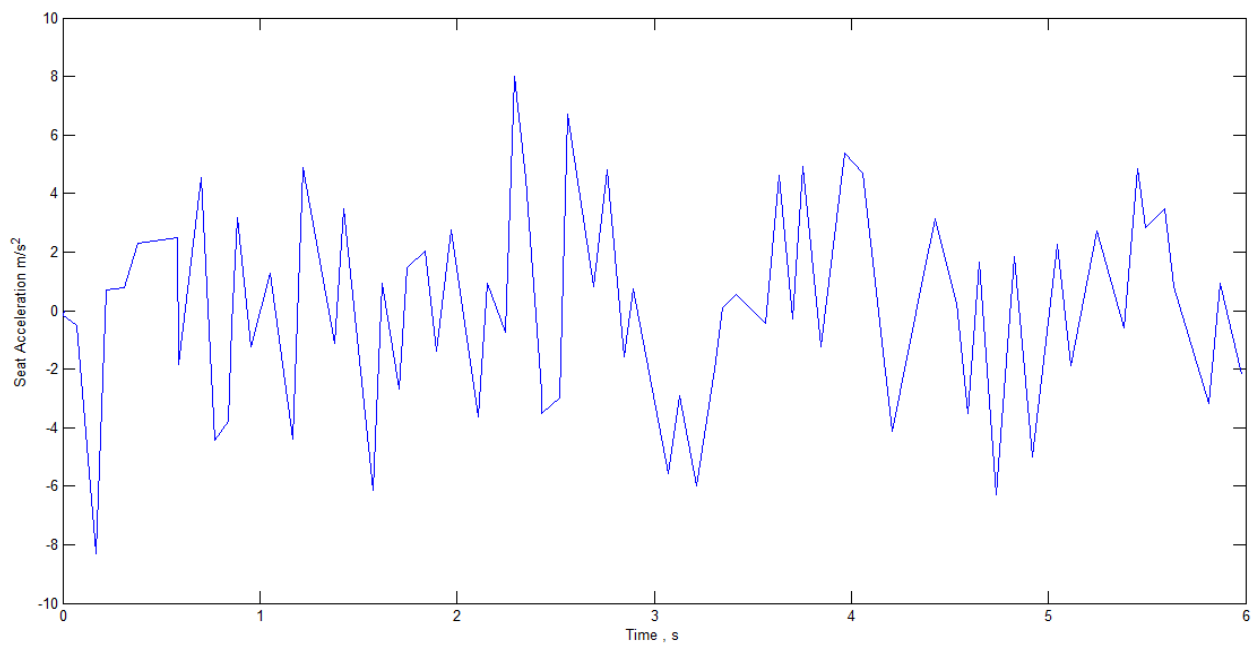


Figure 4.12: Vertical acceleration of the passenger [4]

The max. and min. acceleration values obtained from Simulink scope are -8 to 10 m/s^2 .

The max. and min. values obtained from figure 4-12 is -8 to 8 m/s^2

Force acting on the passenger:

Multiplying the previously obtained passenger acceleration by mass of the passenger (80 kg) [4] we obtain the plot for the force acting on the passenger.

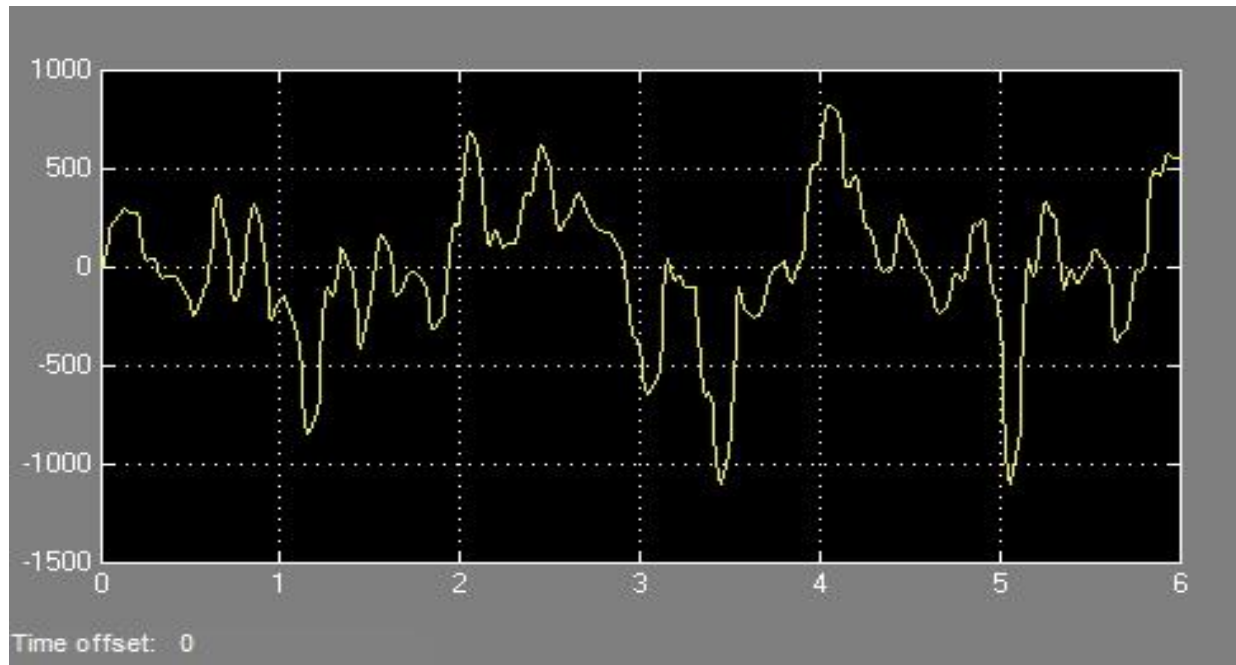


Figure 4.13: Force acting on passenger

Due to the high speed of the motorcycle considered in [4] which is 80 km/h, the rider feels varying forces of magnitudes -1000 N to 800 N approximately.

For the most part the forces are below 500 N, for very short periods rider feels forces of higher magnitudes as is illustrated in the above graph.

4.3 6 DOF Model subjected to realistic speed bumps:

The profile of the speed bump generated in the previous sections is applied to the simulink model.

The front bump acts in the time range 1 to 1.198 sec

the rear bump acts in the time range 1.525 to 1.723 sec,

Both of these inputs act on the system as a whole.

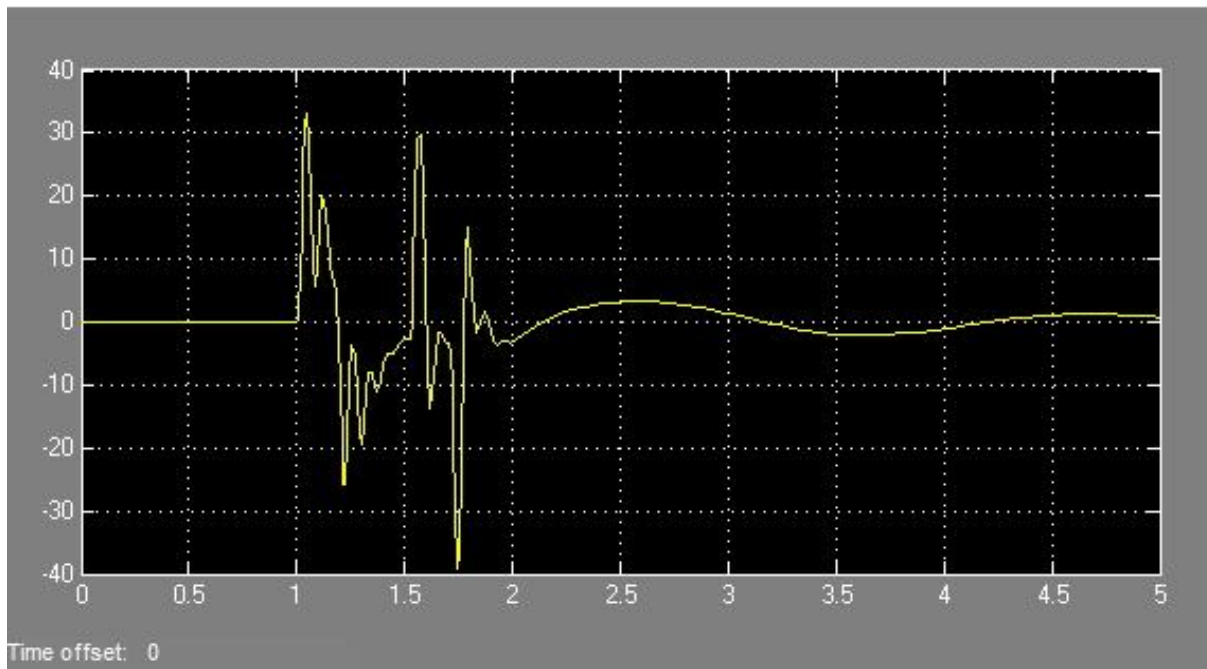


Figure 4.14: Passenger acceleration

The response can be interpreted as 4 zones:

- Response of system when front wheel hits the speed bump: 1 to 1.198 sec
- Response of system when front wheel passes the speed bump: 1.198 to 1.525 sec
- Response of system when rear wheel hits the speed bump: 1.525 to 1.723 sec
- Response of system when rear wheel crosses speed bump: 1.723 sec onwards.

This applies to all the acceleration and force graphs for realistic bump.

After 1.723 sec the system has successfully crossed the speed bump and is reverting back to its normal state. The motorcycle passes over the bump at a constant speed of 10 km/h, it doesn't slow down at the start of the bump hence, the passenger faces considerable vertical acceleration between -30 to 30 m/s².

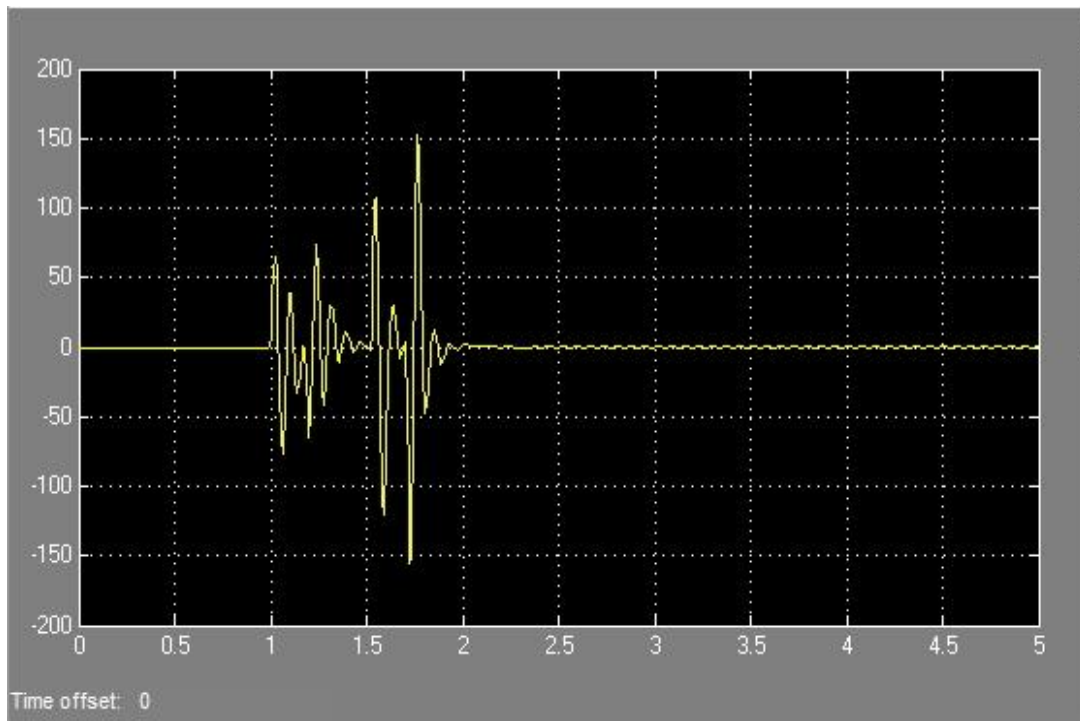


Figure 4.15: Sprung mass acceleration

- The sprung mass faces higher vertical acceleration than that of the passenger.
- It can be said that the sprung mass absorbs most of the speed bump shock. This is the result of being directly connected to the suspension.
- This causes damage to the sprung mass in the long run and causes durability issues such as rattling and unwanted vibrations of the part.
- In between 1.525 to 1.723 sec, the sprung mass faces the largest value of vertical acceleration.
- The sprung mass is already unsettled due to the front wheel hitting the bump when the rear wheel hits the bump. So the sprung mass experiences a strong jerk.
- This is the direct consequence of hitting the speed bump at a constant speed and not slowing down while going over the speed bump.

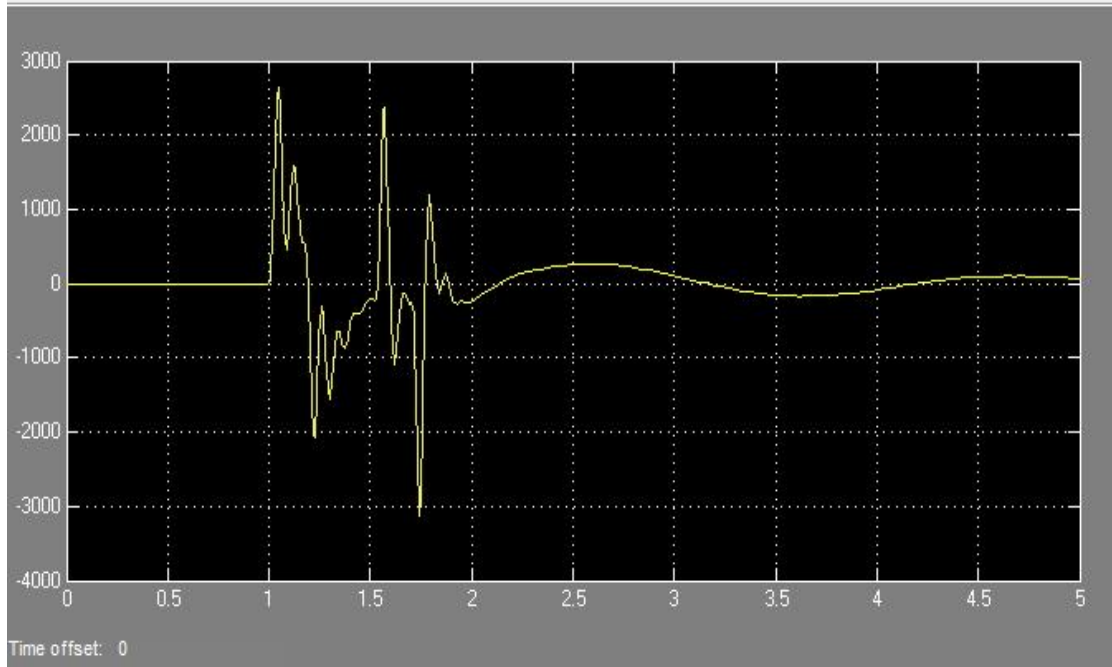


Figure 4.16: Vertical force acting on the passenger

The passenger feels the most upward force when the front wheel passes over the bump. This is due to sudden change in displacement in otherwise uniform motion.

The passenger faces the most downward force when the rear wheel passes over the bump.

This varying nature of forces can cause back problems for the passenger in the long run.

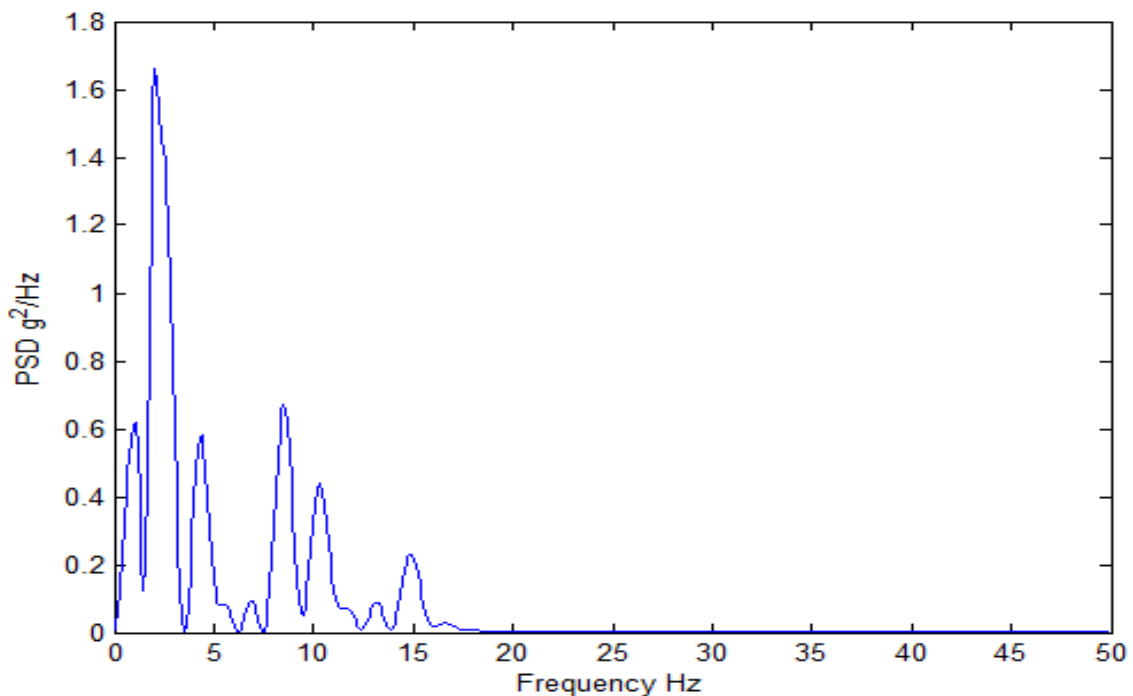


Figure 4.17: PSD for the passenger acceleration for 6 DOF

The acceleration response PSD of motorcycle passenger with realistic bump input has a very distinct peak around 2 Hz.

Also, it is observed from [3], and the frequency of the main peak remains unchanged for varying speeds.

Thus, it is inferred that peak which is around 2 Hz is due to the motorcycle's inherent characteristics.

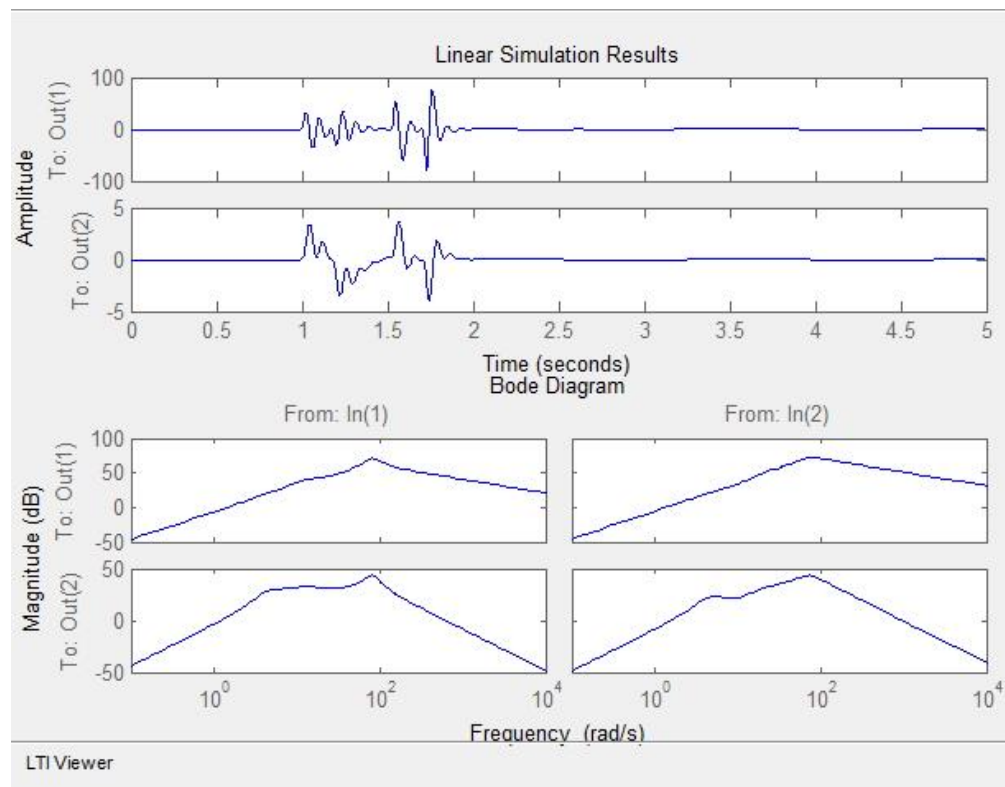


Fig 4.18: lsim and bode plot of bump response

First plot in fig 4.18 represents the lsim plot of the system

Second plot is the bode plot

Bode plot is a log-log plot of the Magnitude response vs frequency.

Advantage of Bode plot is that it shows effect of individual signals on out (1) which is sprung mass and out (2) which represents the rider.

It shows the effect of individual signals on the specific parts of motorcycle such as sprung mass and rider.

4.4: Comparison of 5 DOF and 6 DOF models based on triangular bump PSD:

The data parameters for 5 DOF were not specified in [3], so instead of using 5 DOF data, the data for 6 DOF was used to plot the PSD.

Thus, the PSD of 6 DOF is plotted and compared with the reference 5 DOF.

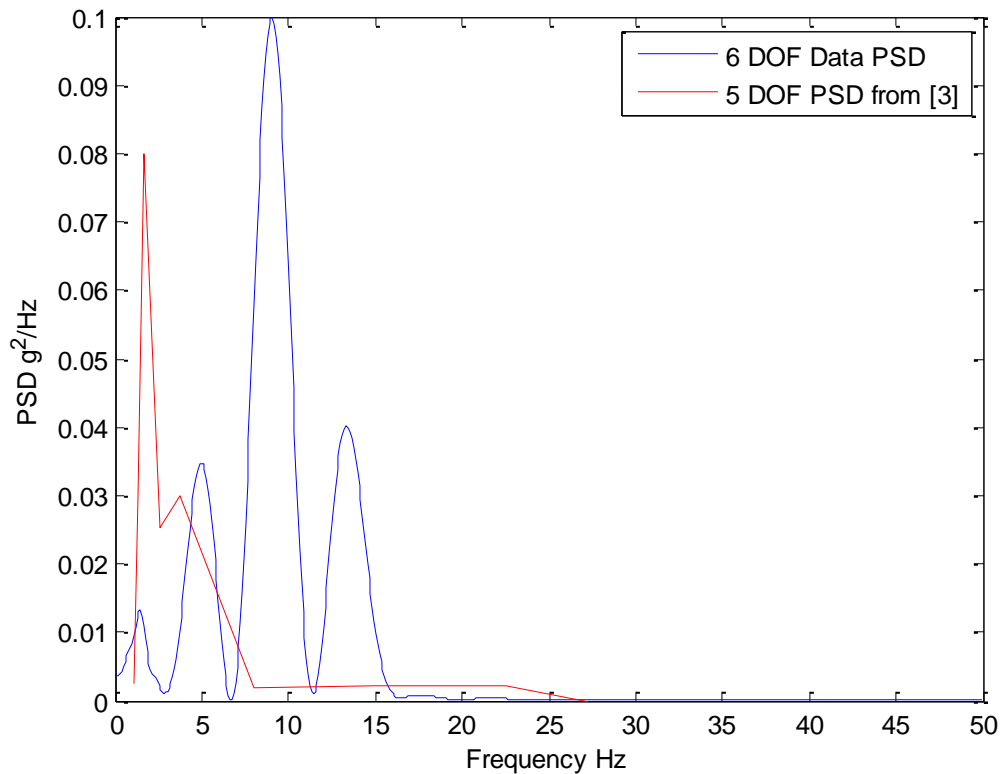


Fig 4.19: Rider PSD for 5 and 6 DOF comparison

There is a variation as the plots are for different data, but still gives a very good idea of the responses for different models

In 5 DOF model [3], the data parameters are not known, therefore, there is a variation.

However, both the 5 DOF and 6 DOF models are simulated for a triangular bump and their PSD are computed.

Chapter 5: Conclusions and Future Work

5.1 Four DOF model:

The front and rear bounce (natural frequency) of the sprung mass values are found. Also the front and rear hop for unsprung masses are found. Also the front and rear hop for unsprung masses are found. The graphs for the same are in agreement with the calculated values.

As the peaks for unsprung masses are evident even in sprung mass graphs, it proves that unsprung masses play important role in determining in-plane comfort.

Thus, the values of unsprung masses should be reduced as much as possible for in-plane comfort.

5.2 Six DOF model on C grade road:

In section 4.2, inputs for C grade road are plotted. It is difficult to compare random data but an effort and a comparison has been made.

Effect of C grade road has been studied on passenger and sprung mass. Since the velocity is high (80 km/h), it can be seen that driving motorcycle at higher velocities causes a lot of vertical acceleration shocks even on normal road surface.

This makes riding experience less comfortable and jerky. Combined with wind blast, high speeds on motorcycle can induce instability despite proper design solely due to road roughness.

5.3 6 DOF model subjected to realistic bump:

A realistic bump of width 55 cm and height 7.5 cm is considered. A constant velocity (10 km/h) of motorcycle is considered. Since, the velocity is constant over the speed bump; it is equivalent to not slowing down over the speed bump.

Not slowing down over speed bump causes high fluctuating shocks to passenger especially on a motorcycle.

From the graphs we can conclude, that driving in this manner can cause rider to develop back problems.

5.4 Comparison of models subjected to triangular bumps:

Comparison of 5 DOF and 6 DOF model proves that even if data is different, PSD of passenger acceleration always has a significant main peak which occurs within the first two peaks.

This power concentration must be optimized to improve passenger comfort.

5.5 Future work:

Building on the work of the thesis, the following work would be helpful in improving rider comfort:

1. Ways to reduce unsprung mass interference in ride comfort
2. Road conditions have a huge influence on motorcycle stability at high speeds. Thus, efforts must be made to improve so said stability issue.
3. Design of speed limiting devices which are less obtrusive than speed breakers and have no long term health effects.
4. Power concentration as seen in PSD plot needs further reduction by optimal suspension design.

References

- [1] Simeon, B., Grupp, F., Führer, C., & Rentrop, P. (1994). A nonlinear truck model and its treatment as a multibody system. *Journal of Computational and Applied Mathematics*, 50(1-3), 523-532.
- [2] Robledo Ricardo, L. (2013). *Nonlinear Stochastic Analysis of Motorcycle Dynamics* (Doctoral dissertation, Rice University).
- [3] Yuan, D. M., Zheng, X. M., & Yang, Y. (2010). Modeling and simulation of motorcycle ride comfort based on bump road. In *Advanced Materials Research* (Vol. 139, pp. 2643-2647). Trans Tech Publications.
- [4] Wu, L., & Zhang, W. J. (2010). Hierarchical modeling of semi-active control of a full motorcycle suspension with six degrees of freedoms. *International Journal of Automotive Technology*, 11(1), 27-32.
- [5] Cossalter, V., Doria, A., Garbin, S., & Lot, R. (2006). Frequency-domain method for evaluating the ride comfort of a motorcycle. *Vehicle System Dynamics*, 44(4), 339-355.
- [6] Zou, X. H., Shi, Q., & Zhang, X. X. (2010). Simulation and Verification on Motorcycle Ride Comfort under Pulse Road. In *Applied Mechanics and Materials* (Vol. 29, pp. 2544-2548). Trans Tech Publications.
- [7] Tyan, F., Hong, Y. F., Tu, S. H., & Jeng, W. S. (2009). Generation of random road profiles. *Journal of Advanced Engineering*, 4(2), 1373-1378.
- [8] Hadpe, M., Deshmukh, D. S., & Solanki, P. M. Vibration Analysis of a Two Wheeler (Analytically).
- [9] Hadpe, M., Deshmukh, D. S., & Solanki, P. M. Vibration Analysis of a Two Wheeler (Analytically).
- [10] Kuber, C. (2014). Modelling Simulation And Control of an Active Suspension System. *International Journal of Mechanical Engineering & Technology (IJMET)*, 5(11), 66-75.
- [11] Jin, L., Yu, Y., & Fu, Y. (2016). Study on the ride comfort of vehicles driven by in-wheel motors. *Advances in Mechanical Engineering*, 8(3), 1687814016633622.

- [12] Feng, J., Zhang, X., Guo, K., Ma, F., & Karimi, H. R. (2013). A frequency compensation algorithm of four-wheel coherence random road. *Mathematical Problems in Engineering*, 2013.
- [13] Rao, L. G., & Narayanan, S. (2008). Preview control of random response of a half-car vehicle model traversing rough road. *Journal of sound and vibration*, 310(1), 352-365.
- [14] Soman, S., Shaji, S., Thomas, V. T., Vishnu, E. M., & Varghese, A. K. (2015). Semi-Active Suspension for Two Wheelers. *International Journal for Innovative Research in Science and Technology*, 1(11), 66-71.
- [15] Weiguo, W., Teng, J., & Furui, X. (2015). Numerical simulation and statistical analysis of random response of the landing gear at taxiing.
- [16] Yonglin, Z., Honghua, T., & Chuanliang, H. (2005). Research and design of time domain simulation system for vehicle road stochastic irregularity. *Transactions of the CSAE*, 21(2), 86-91.
- [17] Peng, B. B., & Huang, X. Q. (2006, December). A simulation test method for a half semi-active vehicle suspension based on the hierarchical modeling method. In *Vehicular Electronics and Safety, 2006. ICVES 2006. IEEE International Conference on* (pp. 63-67). IEEE.
- [18] Pacejka, H. B., & Bakker, E. (1992). The magic formula tyre model. *Vehicle system dynamics*, 21(S1), 1-18.
- [19] Cossalter, V., Da Lio, M., & Lot, R. (1995). Mathematical modelling of two-wheeled vehicles.
- [20] Patil, M. K., Palanichamy, M. S., & Ghista, D. N. (1978). Man-tractor system dynamics: towards a better suspension system for human ride comfort. *Journal of biomechanics*, 11(8-9), 397-406.
- [21] Cossalter, V., Doria, A., & Lot, R. (2000). Optimum suspension design for motorcycle braking. *Vehicle system dynamics*, 34(3), 175-198.
- [22] Cossalter, V., Aguggiaro, A., Debus, D., Bellati, A., & Ambrogi, A. (2007, June). Real cases motorcycle and rider race data investigation: Fall behavior analysis. In *Proc. of 20th Enhanced Safety of Vehicles Conference, Innovations for Safety Opportunities and Challenges*

Lyon.

[23] < <http://www.portlandoregon.gov/transportation/35934?a=85397>>

[24] Cossalter, V. (2006). Motorcycle dynamics. Lulu. com.

[25] Hatch, M. R. (2000). Vibration simulation using MATLAB and ANSYS. CRC Press.

[26] <<http://www.hemmings.com/magazine/hsx/2010/06/1894-Hildebrand--amp--Wolfm-uuml-ller-Recreation/3333961.html>>

[27] <http://newautomotivewallpapers.com/2016-yamaha-yzf-r1-wallpapers.html>>

[28] <<http://www.motorcycle-usa.com/81957/buyers-guide-specs/2016-harley-davidson-sportster-iron-883/>>

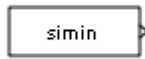
[29] < <http://www.topspeed.com/motorcycles/motorcycle-reviews/husqvarna/2016-husqvarna-fe-450-fe-501-fe-501-s-ar170878.html>>

[30] < <http://www.trench-covers.co.uk/modular-speed-bump-system>>

[31] < <https://brentwood-tn.org/index.aspx?page=215>>

Appendix:

Type of Simulink model blocks used for modelling:



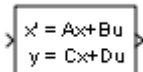
1.

The simin or from workspace block is used to import data from the Matlab workspace. This input is imported from Matlab workspace. The front and rear inputs for C grade road are also generated using Simulink and are explained in the further sections.



2.

The 'Mux' block combines its input into a single output, but it retains the individuality. All inputs must be of same data type and have an equal number of timesteps.



3.

The state space block implements a system whose behaviour is defined as

$$\dot{x} = Ax + Bu$$

$$y = Cx + Du$$

x is the state vector and y represents the output.

4.



The 'Demux' block extracts the component of an input signal and outputs the component as separate signals. It basically splits the combined signal into required outputs.



5.

The 'Gain' block multiplies the input by a constant value (gain). In the above model, the gain block is used to multiply mass so as to find force spectrum.

6.



The Simulink 'Scope' block displays time domain signals with respect to simulation time. The scope block is used to verify that the input is of the desired nature and is present at each stage of output operations.

analysis of motorcycle model for road bumps

ORIGINALITY REPORT

10%	5%	7%	4%
SIMILARITY INDEX	INTERNET SOURCES	PUBLICATIONS	STUDENT PAPERS

PRIMARY SOURCES

1	www.mathworks.com Internet Source	1%
2	Submitted to Oxford Brookes University Student Paper	1%
3	Chen, Wuwei, Hansong Xiao, Qidong Wang, Linfeng Zhao, and Maofei Zhu. "Vertical Vehicle Dynamics and Control", Integrated Vehicle Dynamics and Control, 2016. Publication	<1%
4	Long Wu. "A HIL simulation experiment design based on a hierarchical modelling method", International Journal of Vehicle Autonomous Systems, 2007 Publication	<1%
5	Submitted to De Montfort University Student Paper	<1%
6	en.wikipedia.org Internet Source	<1%